Inorg. Chem. **2004**, *43*, 5572–5587

Synthesis, Characterization, and X-ray Crystal Structures of Cyclam Derivatives. 5. Copper(II) Binding Studies of a Pyridine-Strapped 5,12-Dioxocyclam-Based Macrobicycle[1]

Michel Meyer,[†] Laurent Frémond,[†] Enrique Espinosa,[†] Roger Guilard,*[,†] Zhongping Ou,[‡] and Karl M. Kadish[‡]

Laboratoire d'Ingénierie Moléculaire pour la Séparation et les Applications des Gaz (LIMSAG, UMR 5633 du CNRS), Université de Bourgogne, Faculté des Sciences, 6 boulevard Gabriel, 21100 Dijon, France, and Department of Chemistry, University of Houston, Houston, Texas 77204-5641

Received April 13, 2004

The copper(II) binding properties of the macrobicyclic diamide 1,9,12,18,22-pentaazatricyclo[7.6.6.1^{3,7}]docosa-3,5,7-(22)-triene-13,19-dione (**L^1**) have been fully investigated by spectroscopic (IR, UV–vis, EPR, MALDI-TOF MS), X-ray diffraction, potentiometric, electrochemical, and spectroelectrochemical methods. This constrained receptor possesses a hemispherical cavity created by cross-bridging the 1 and 8 positions of *trans*-dioxocyclam (1,4,8,11-tetraazacyclotetradecane-5,12-dione, **L^2**) with a 2,6-pyridyl strap. Treatment of **L^1** with a copper salt in methanol produces a red complex of [Cu(**L^1**H$_{-1}$)]$^+$ formula in which the copper atom is embedded in a 13-membered ring and coordinated by both amines as well as the pyridine and one deprotonated amide nitrogen atoms. Infrared spectroscopy provides evidence for protonation of the carbonyl oxygen atom belonging to the copper-bound amide of [Cu(**L^1**H$_{-1}$)]$^+$ under strongly acidic conditions. The resulting conversion of the amidate into an iminol group highlights the inert character of the corresponding complexes, which do not dissociate at low pH values. In contrast, both secondary amides of **L^1** deprotonate in the presence of a weak base, thus affording a blue pentacoordinated [Cu(**L^1**H$_{-2}$)] compound where the copper atom sits in the center of the 14-membered dioxocyclam fragment. In aqueous solution, both complexes undergo a pH-driven ($pK_a = 8.73(2)$) molecular reorganization, which is reminiscent of a glider motion. The copper(II) cation switches rapidly and reversibly from a four-coordinate flattened tetrahedral arrangement of the donor atoms in the red species to a five-coordinate environment in the blue species, which is intermediate between a square pyramid and a trigonal bipyramid. Conversion of the red to the blue form was also demonstrated to occur upon reduction of [Cu(**L^1**H$_{-1}$)]$^+$ by cyclic voltammetry ($E_{pc} = -0.64$ V/SCE in CH_3CN).

Introduction

The quest for new macropolycyclic receptors that could serve as functional catalysts or as models of biological systems is stimulating continuous endeavor, and considerable efforts have been invested over the past decades in the design of new synthetic strategies. In that respect, conformationally constrained bicyclic polyamines have gained increasing interest since they exhibit intriguing anion, proton, and metal coordination properties.[2−9] Morevover, cryptand-like peptides have served as structural probes for mapping the binding characteristics of various biological receptors.[10]

* Author to whom correspondence should be addressed. E-mail: Roger.Guilard@u-bourgogne.fr. Phone: (33) 3 80 39 61 11. Fax: (33) 3 80 39 61 17.

[†] Université de Bourgogne.

[‡] University of Houston.

(1) For the previous paper in this series, see: Frémond, L.; Espinosa, E.; Meyer, M.; Denat, F.; Guilard, R.; Huch, V.; Veith, M. *New J. Chem.* **2000**, *24*, 959.
(2) Alder, R. W. *Chem. Rev.* **1989**, *89*, 1215.
(3) Alder, R. W. *Tetrahedron* **1990**, *46*, 683.
(4) Dietrich, B.; Viout, P.; Lehn, J. M. *Macrocyclic Chemistry*; VCH: Weinheim, Germany, 1993.
(5) Nelson, J.; McKee, V.; Morgan, G. *Prog. Inorg. Chem.* **1998**, *47*, 167.
(6) Bencini, A.; Bianchi, A.; Garcia-Espana, E.; Micheloni, M.; Ramirez, J. A. *Coord. Chem. Rev.* **1999**, *188*, 97.
(7) Ingham, A.; Rodopoulos, M.; Coulter, K.; Rodopoulos, T.; Subramanian, S.; McAuley, A. *Coord. Chem. Rev.* **2002**, *233−234*, 255.
(8) Hubin, T. J. *Coord. Chem. Rev.* **2003**, *241*, 27.
(9) Springborg, J. *Dalton Trans.* **2003**, 1653.
(10) Virta, P.; Lönnberg, H. *J. Org. Chem.* **2003**, *68*, 8534.

10.1021/ic049518k CCC: $27.50
Published on Web 08/06/2004

Chart 1

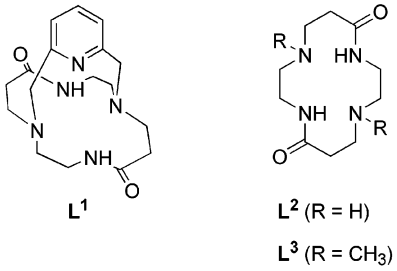

L^1 L^2 (R = H) L^3 (R = CH_3)

Dioxocyclams are 14-membered tetraazacycloalkanes in which amide groups replace two out of four secondary amines. Their structure is therefore intermediate between the corresponding saturated tetraamine 1,4,8,11-tetraazacyclotetradecane, the so-called cyclam, and oligopeptides.[11,12] *trans*-Dioxocyclams have the carbonyl groups disposed in position 5 and 12 and can therefore be viewed as trans "autodiprotected" cyclam building blocks.[13] Several representatives have been described in the literature, although the parent compound, 1,4,8,11-tetraazacyclotetradecane-5,12-dione (**L²**), better known under its short name 5,12-dioxocyclam (Chart 1), has received much less attention compared to its other isomers probably because the synthetic procedure has been originally reported in a patent by Tomalia and Wilson.[14] Despite the low yield (∼2%) of the [2 + 2] Michael reaction, 100-g amounts of 5,12-dioxocyclam can be straightforwardly isolated using standard laboratory glassware equipments.[1] More recently, Hegedus and coworkers obtained C-functionalized, optically active analogues starting from chromium carbene complexes.[15−18] Their photolysis in the presence of suitable imidazolines produces a series of azapenams, which dimerize under acidic reductive conditions to afford the desired compounds.

Besides its ability to bind some transition metals in a square-planar environment,[19,20] 5,12-dioxocyclam can be regarded as a highly valuable starting material for the preparation of 1,8-disubstituted cyclam-based ligands[13,21] and more interestingly provides a convenient entry into a new and highly preorganized class of receptors possessing well-defined but tunable metal-binding cavities. Provided the synthon is reacted with the appropriate biselectrophile, macrobicyclic and macrotricyclic cages of spheroidal and cylindrical topologies can easily be obtained (Chart 1).[22−26] Hegedus prepared analogous capped and bridged C-substituted 5,12-dioxocyclams and some of their metal complexes using copper or nickel.[17,27−33] Paradoxically, this class of compounds has not been subject to detailed physicochemical investigations[23] although some ligands in their free or complexed state have been structurally characterized by X-ray diffraction.[29−33] We present herein the copper(II) binding properties of the *ansa*-pyridine 5,12-dioxocyclam derivative **L¹** (Chart 1), which have been studied by means of spectroscopic, structural, thermodynamic, and electrochemical methods.

Results and Discussion

Synthesis and FTIR Spectroscopy of $[Cu(L^1H_{-1})]ClO_4\cdot H_2O$. Treatment of **L¹** with stoichiometric amounts of $CuClO_4\cdot 6H_2O$ dissolved in methanol leads to a green solution which progressively turns dark-red upon stirring at room temperature. After 4 days, the complex was recovered as a powder by evaporation of the solvent. Recrystallization in water afforded violet-red crystals of $[Cu(L^1H_{-1})]ClO_4\cdot H_2O$ formula as suggested by elemental CHN analysis. The corresponding triflate and thiocyanate salts were isolated following the same procedure.

The different complexes give rise to similar infrared spectra, which differ only by the characteristic vibration bands of the cocrystallized anions: $\nu_3 = 1093$ cm^{-1} and $\nu_4 = 624$ cm^{-1} for the perchlorates; $\nu_{SO_3asym} = 1266$ cm^{-1}, $\nu_{CF_3sym} = 1227$ cm^{-1}, $\nu_{SO_3sym} = 1030$ cm^{-1}, and $\delta_{SO_3sym} = 637$ cm^{-1} for the triflates;[34] $\nu_{C\equiv N} = 2064$ and 2075 cm^{-1} for the thiocyanates.[35] Two resolved absorptions at 3580 and 3510 cm^{-1} confirm the presence of the cocrystallized, hydrogen-bonded water molecule found by combustion analysis. Stretching and bending modes ($\nu_{C=O} = 1666$ cm^{-1} and $\delta_{CNH} = 1535$ cm^{-1}) associated with the amide functionalities are observed at frequencies similar to those found for the free ligand ($\nu_{C=O} = 1654$ cm^{-1} and $\delta_{CNH} = 1526$ cm^{-1}), which suggests the presence of an uncoordinated amide group. In addition, a third band, which is more intense than the pyridine-centered $\nu_{C=C}$ and $\nu_{C=N}$ elongation modes appearing at 1574 cm^{-1} in the free ligand spectrum, occurs at 1581 cm^{-1} in the case of the complex and thus partially obscures the aromatic-ring absorptions. Both the position and the intensity of this feature are compatible with the data

(11) Kimura, E. *J. Coord. Chem.* **1986**, *15*, 1.
(12) Sigel, H.; Martin, R. B. *Chem. Rev.* **1982**, *82*, 385.
(13) Denat, F.; Brandès, S.; Guilard, R. *Synlett* **2000**, 561.
(14) Tomalia, D. A.; Wilson, L. R. U.S. Patent 4 517 122, 1985.
(15) Betschart, C.; Hegedus, L. S. *J. Am. Chem. Soc.* **1992**, *114*, 5010.
(16) Hegedus, L. S.; Moser, W. H. *J. Org. Chem.* **1994**, *59*, 7779.
(17) Hsiao, Y.; Hegedus, L. S. *J. Org. Chem.* **1997**, *62*, 3586.
(18) Hegedus, L. S.; Greenberg, M. M.; Wendling, J. J.; Bullock, J. P. *J. Org. Chem.* **2003**, *68*, 4179.
(19) Frémond, L. Ph.D. Thesis, Université de Bourgogne, Dijon, France, 2002.
(20) Gavrish, S. P.; Lampeka, Y. D.; Lightfoot, P. *Inorg. Chim. Acta* **2004**, *357*, 1023.
(21) Goeta, A. E.; Howard, J. A. K.; Maffeo, D.; Puschmann, H.; Williams, J. A. G.; Yufit, D. S. *J. Chem. Soc., Dalton Trans.* **2000**, 1873.
(22) Denat, F.; Lacour, S.; Brandès, S.; Guilard, R. *Tetrahedron Lett.* **1997**, *38*, 4417.
(23) Brandès, S.; Denat, F.; Lacour, S.; Rabiet, F.; Barbette, F.; Pullumbi, P.; Guilard, R. *Eur. J. Org. Chem.* **1998**, 2349.
(24) Plenio, H.; Aberle, C. *Chem. Commun.* **1998**, 2697.
(25) Plenio, H.; Aberle, C.; Shihadeh, Y. A.; Lloris, J. M.; Martinez-Manez, R.; Pardo, T.; Soto, J. *Chem.—Eur. J.* **2001**, *7*, 2848.
(26) Hubin, T. J.; Tyryshkin, N.; Alcock, N. W.; Busch, D. H. *Acta Crystallogr., Sect. C* **1999**, *55*, 1888.
(27) Dumas, S.; Lastra, E.; Hegedus, L. S. *J. Am. Chem. Soc.* **1995**, *117*, 3368.
(28) Kuester, E.; Hegedus, L. S. *Organometallics* **1999**, *18*, 5318.
(29) Puntener, K.; Hellman, M. D.; Kuester, E.; Hegedus, L. S. *J. Org. Chem.* **2000**, *65*, 8301.
(30) Wynn, T.; Hegedus, L. S. *J. Am. Chem. Soc.* **2000**, *122*, 5034.
(31) Brugel, T. A.; Hegedus, L. S. *J. Org. Chem.* **2003**, *68*, 8409.
(32) Hegedus, L. S.; Sundermann, M. J.; Dorhout, P. K. *Inorg. Chem.* **2003**, *42*, 4346.
(33) Achmatowicz, M.; Hegedus, L. S.; David, S. *J. Org. Chem.* **2003**, *68*, 7661.
(34) Johnston, D. H.; Shriver, D. F. *Inorg. Chem.* **1993**, *32*, 1045.
(35) Nakamoto, K. *Infrared and Raman Spectra of Inorganic and Coordination Compounds*; Wiley: New York, 1970.

Table 1. X-ray Crystallographic Data for $[Cu(\mathbf{L^1}H_{-1})]ClO_4 \cdot H_2O$ and $[Cu(\mathbf{L^1}H_{-2})] \cdot 4H_2O$

	$[Cu(\mathbf{L^1}H_{-1})]ClO_4 \cdot H_2O$	$[Cu(\mathbf{L^1}H_{-2})] \cdot 4H_2O$
empirical formula	$C_{17}H_{26}ClCuN_5O_7$	$C_{17}H_{31}CuN_5O_6$
fw	511.42	465.01
space group	$P2_12_12_1$ (No. 19)	$C2/c$ (No. 15)
a, Å	8.0150(3)	20.0210(8)
b, Å	13.6120(5)	12.1560(5)
c, Å	18.6620(6)	16.5210(6)
β, deg	90	91.303(2)
V, Å^3	2036.0(1)	4019.8(3)
Z	4	8
T, K	110(2)	110(2)
ρ_{calcd}, g cm^{-3}	1.668	1.537
μ(Mo Kα), mm^{-1}	1.256	1.132
R indices [$I > 2\sigma(I)$][a]	$R_1 = 0.0413$; $wR_2 = 0.0927$	$R_1 = 0.0537$; $wR_2 = 0.1081$
R indices (all data)[a]	$R_1 = 0.0543$; $wR_2 = 0.0992$	$R_1 = 0.0884$; $wR_2 = 0.1247$

[a] $R_1 = \sum||F_o| - |F_c||/\sum|F_o|$, $wR_2 = \{\sum[w(F_o^2 - F_c^2)^2]/\sum[w(F_o^2)^2]\}^{1/2}$.

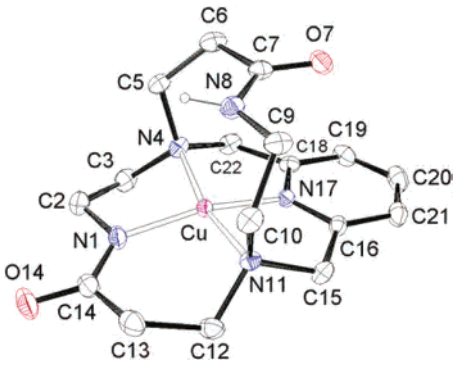

Figure 1. ORTEP view of the structure of $[Cu(\mathbf{L^1}H_{-1})]ClO_4 \cdot H_2O$ showing the atom-labeling scheme and the thermal ellipsoids at the 50% probability level. All H(−C) hydrogen atoms, the counterion, and the water molecule have been omitted for clarity.

reported for copper-bound carboxamido nitrogen atoms.[11,36,37] A literature survey shows that the metal-assisted deprotonation of primary and secondary amides typically results in a ca. 80−100 cm^{-1} bathochromic shift of the carbonyl stretching frequency ($\nu_{C=O}$). Hence, the second amide group contained in the dioxocyclam subunit is expected to coordinate the copper(II) center through a negatively charged nitrogen atom, giving rise to a singly positively charged complex.

X-ray Crystal Structure of $[Cu(\mathbf{L^1}H_{-1})]ClO_4 \cdot H_2O$. To provide final proof of the stoichiometry and connectivity derived from the elemental analysis, mass, and IR spectroscopic data, a crystallographic study of the copper(II) complex has been carried out. Good X-ray quality, violet-red single crystals of parallelepipedic shape were grown from an aqueous solution of the perchlorate salt by slow evaporation at room temperature. Diffraction conditions and crystal and refinement data are summarized in Table 1. The structure consists of discrete $[Cu(\mathbf{L^1}H_{-1})]^+$ cations, perchlorate anions, and hydrogen-bonded water molecules. The ORTEP view of the cationic complex reproduced in Figure 1 displays a single deprotonated amide group ligated to Cu^{2+} via N1 (Table 2), whereas the second amide function remains unbound to the metal (Cu···N8 = 2.575(2) Å), adopting a stable Z conformation. As a consequence, the 14-membered dioxocyclam ring is folded along the virtual axis passing through the pivotal bridgehead tertiary amines N4 and N11 by an angle of 112.1°, which corresponds to the dihedral angle Ω_{14} between the planes (N1, N4, N11) and (N8, N4, N11).[38] This folding enables the N17 pyridine nitrogen atom to complete the coordination sphere (N1−Cu−N17 = 157.4(1)°; N4−Cu−N11 = 167.2(1)°), which is strapped by the unbound β-alaninamide fragment disposed like the handle above a basket.

According to this arrangement, the copper cation is encapsulated inside a cyclic structure composed of 13 atoms and sits 0.10 Å below the least-squares plane defined by the four N1, N4, N11, N17 donors. In turn, the nitrogen atoms deviate in an alternate fashion by ±0.24(1) Å from the N_4 coordination plane, which is almost coplanar with the aromatic ring (dihedral angle = 6.7°) and the free amide moiety (dihedral angle = 3.2°). The metal takes part in three five-membered and one six-membered chelate rings with

Table 2. Selected Bond Distances (Å) and Angles (deg) for $[Cu(\mathbf{L^1}H_{-1})]ClO_4 \cdot H_2O$ and $[Cu(\mathbf{L^1}H_{-2})] \cdot 4H_2O$

		$[Cu(\mathbf{L^1}H_{-2})]$	
	$[Cu(\mathbf{L^1}H_{-1})]^+$	stereoisomer A	stereoisomer B
Cu−N1	1.877(2)	1.950(4)	1.95(1)
Cu−N4	2.028(2)	2.030(2)	2.022(2)
Cu−N8	2.575[a]	1.962(3)	2.01(1)
Cu−N11	2.009(2)	2.022(2)	2.030(2)
Cu−N17	1.885(2)	1.997(2)	1.997(2)
N1−C14	1.312(4)	1.309(6)	1.31(2)
C14−O14	1.267(3)	1.267(6)	1.27(2)
N8−C7	1.354(3)	1.302(5)	1.30(2)
C7−O7	1.235(3)	1.266(8)	1.29(3)
N1−Cu−N4	89.4(1)	87.8(1)	
N1−Cu−N8	113.8[a]	130.4(2)	135.4(5)
N1−Cu−N11	102.4(1)	99.8(1)	
N1−Cu−N17	157.4(1)	116.5(1)	114.1(4)
N4−Cu−N8	90.8[a]	100.1(1)	
N4−Cu−N11	167.21(9)	163.8(1)	163.8(1)
N4−Cu−N17	84.67(9)	81.53(9)	82.3(1)
N8−Cu−N11	80.0[a]	86.0(1)	
N8−Cu−N17	88.1[a]	113.1(1)	110.5(3)
N11−Cu−N17	86.18(9)	82.3(1)	81.53(9)

[a] N8 is not bonded to the copper atom in $[Cu(\mathbf{L^1}H_{-1})]^+$; the metrical parameter is only given for information purposes.

(36) Kimura, E.; Koike, T.; Machida, R.; Nagai, R.; Kodama, M. *Inorg. Chem.* **1984**, *23*, 4181.
(37) Siegfried, L.; Neuburger, M.; Zehnder, M.; Kaden, T. A. *J. Chem. Soc., Chem. Commun.* **1994**, 951.
(38) Costa, J.; Delgado, R.; Drew, M. G. B.; Félix, V.; Saint-Maurice, A. *J. Chem. Soc., Dalton Trans.* **2000**, 1907.

N−Cu−N bite angles close to 90° for the former and 100° for the latter (Table 2). A puckering analysis was undertaken to provide a detailed conformational description for each individual chelate ring.[39] Accordingly, the ethylenediamine Cu−N1−C2−C3−N4 subunit adopts an envelope arrangement where C3 is out of the mean plane (Q = 0.449 Å; φ = 116.7°). For both adjacent Cu−N4−C22−C18−N17 and Cu−N11−C15−C16−N17 fragments containing the pyridine moiety, the closest pucker descriptor is a half-chair twisted along N4−C22 (Q = 0.192 Å; φ = 227.9°) and N11−C15 (Q = 0.168 Å; φ = 58.8°), respectively. Finally, the six-membered chelate ring is strongly distorted (Q = 0.478 Å; θ = 47.6°; φ = 250.3°) due to the planarity of the amidato group imposed by resonance and thus adopts an intermediate geometry between a half-chair (θ = 50.8°; φ = 270°) and an envelope on C12 (θ = 54.7°; φ = 240°). In this way, the spatial arrangement adopted by the backbone minimizes the steric repulsion between hydrogen atoms, as both ethane chains belonging to the five- and six-membered chelate rings exhibit staggered CH_2 groups. Together with the small value taken by the folding angle Ω_{13} (Ω_{13} = 29.0°) defined as the dihedral angle between the (N1, N4, N11) and (N17, N4, N11) planes,[38] these results clearly indicate that the cross-bridged macrobicyclic framework allows enough flexibility to accommodate a copper ion preferentially in the 13- rather than in the 14-membered planar cavity.[40]

The degree of distortion of the CuN_4 coordination polyhedron from an ideal planar arrangement of the donor set is best described by the deformation parameter ω corresponding to the dihedral angle between both (N1, Cu, N4) and (N11, Cu, N17) planes.[41] For compressed tetragonal geometries intermediate between the planar and tetrahedral limits, ω increases monotonically from 0 to 90° upon twisting both planes. The ω angle value of 22.7(1)° indicates a strong tetrahedral flattening which results from a balance between crystal field stabilization favoring a square-planar geometry and steric constrains imposed by the macrobicyclic skeleton.

As expected, the $Cu-N_{amidate}$ (1.877(2) Å) and $Cu-N_{pyridine}$ bond lengths (1.885(2) Å) are significantly shorter than $Cu-N_{amine}$ distances (2.009(2) and 2.028(2) Å). Resonance stabilization of the negatively charged peptidic nitrogen atom N1 by electron delocalization induces a more than 0.04 Å shortening of the amidato C−N bond compared to the uncoordinated amide moiety (C14−N1 = 1.312(4) Å vs C7−N8 = 1.354(3) Å). For the same reason, there is a concomitant lengthening of the C−O bond (C14−O14 = 1.267(3) Å vs C7−O7 = 1.235(3) Å), which translates in the infrared spectrum by a 86 cm^{-1} shift of the carbonyl stretching frequency. In addition, the C7−O7 distance is slightly shorter than the corresponding bond length previously reported for **L²** (C−O = 1.264(2) Å).[1] Examination of the crystal packing indicates that the O7 carbonyl oxygen atom, located at 3.16 Å from the center of the pyridine ring, interacts with the cocrystallized water molecule (Ow···O7 = 2.818(3) Å; Ow−Hw1···O = 164(4)°), while the amidic hydrogen atom H8 is engaged in a hydrogen bonding interaction with the amidato O14 oxygen atom belonging to an adjacent complex (N8···O14 = 2.761(3) Å; N8−H8···O14 = 169(3)°).

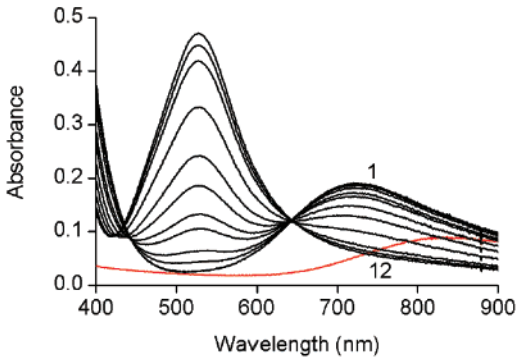

Figure 2. Evolution of the visible absorption spectrum as a function of time for the formation of the copper(II) complexes with **L¹** in methanol without added base. $[Cu^{2+}]_{tot}$ = 4.88 mM, $[\mathbf{L^1}]_{tot}$ = 5.04 mM, T = 25 °C, and l = 1 cm. Spectra 1−12: t = 0.5, 0.7, 5.2, 14.7, 54.5, 95.4, 214.9, 500.2, 1386.3, 3114.2, 4349.1, 5751.8 min after the reaction start (~30 s mixing time). The red line corresponds to the spectrum of a pure 4.88 mM $Cu(CF_3SO_3)_2$ solution in methanol.

Spectroscopic Characterization of the Green Intermediate. Once the structure of the final reaction product was established, identification of the intermediate green species that forms immediately after mixing the reagents was undertaken. To that end, the metalation reaction of **L¹** by anhydrous $Cu(CF_3SO_3)_2$ dissolved in methanol was monitored by visible absorption spectroscopy over a 4-day period until reaching completion (Figure 2). Noteworthy, the first spectrum recorded after stirring the reaction mixture for ~30 s shows a maximum at 719 nm (ϵ = 38 M^{-1} cm^{-1}), which is shifted by ca. 120 nm to higher energies with respect to absorption peak corresponding to the pure copper(II) triflate salt in methanol. Since the free ligand does not absorb in the visible range, these spectroscopic features evidence the rapid formation during the mixing time of a green intermediate complex, which is too fast to be studied by classical spectrophotometry. The absence of clearly defined isosbestic points around 450 nm (Figure 2) suggests that the slow rearrangement process of this intermediate occurs according to a multistep process leading to the final violet-red species, characterized by a d → d absorption maximum centered at 528 nm. Addition during the initial stage of the reaction of a large excess of diethyl ether to the methanolic mixture of **L¹** and $CuClO_4 \cdot 6H_2O$ enabled us to isolate the transient species, which precipitated out as a pale-green powder. Positive MALDI-TOF mass-spectrometric analysis of this solid showed a manifold at m/z = 394, displaying the correct line shape with the expected isotopic distribution for a mononuclear complex with 1:1 ligand-to-metal stoichiometry.

Identification of the green intermediate as a reactive metal−ligand adduct that rearranges to the final red complex was also ascertained by the presence in the infrared spectrum of the characteristic amide bands arising from the **L¹** skeleton (ν_{NH} = 3224 and 3174 cm^{-1}) and the coprecipitated perchlorate anions (ν_3 = 1091 cm^{-1} and ν_4 = 626 cm^{-1}).[35]

(39) Cremer, D.; Pople, J. A. *J. Am. Chem. Soc.* **1975**, *97*, 1354.
(40) Félix, V.; Costa, J.; Delgado, R.; Drew, M. G. B.; Duarte, M. T.; Resende, C. *J. Chem. Soc., Dalton Trans.* **2001**, 1462.
(41) Murakami, Y.; Matsuda, Y.; Sakata, K. *Inorg. Chem.* **1971**, *10*, 1728.

Structural insights about the nature of this initial species could be extracted from the 1500−1700 cm^{-1} region where the $\nu_{C=O}$ vibration frequency is diagnostic for the level of π-electron delocalization.[42,43] By comparison with the spectrum recorded for the free ligand and $[Cu(\mathbf{L^1}H_{-1})]ClO_4 \cdot H_2O$, the strong feature appearing at 1665 cm^{-1} can readily be assigned to the resonance of a free amide carbonyl group.[44] The main difference lies however in the appearance of a new, bathochromically shifted signal with a maximum at 1616 cm^{-1}, partially obscuring the δ_{CNH} bending mode. This energy compares well with the value reported by Kim and Martell ($\nu_{C=O}$ = 1625 cm^{-1}) for the (di-, (tri-, and (tetraglycinato)copper(II) complexes formed at pH ∼ 4 in D_2O solutions.[45,46] Although these authors initially misinterpreted their data, it was later ascertained that this band arises from the metal-coordinated peptide carbonyl oxygen atom.[47−49] Because of the resonance, the formation of a deprotonated nitrogen−copper bond would weaken much more the force constant of the carbonyl stretch of a $O-C-N^-$ system[11,36,37] and would result in a shift of the $\nu_{C=O}$ absorptions from ∼1670 to ∼1580 cm^{-1} as observed for the final product $[Cu(\mathbf{L^1}H_{-1})]ClO_4 \cdot H_2O$. Thus, infrared spectroscopy add strong supporting evidence for a single $-NHC{=}O\cdots Cu$ interaction during the initial stage of the reaction between $\mathbf{L^1}$ and Cu^{2+} rather than for a metal-assisted ionization of the peptide NH function. Moreover, early participation of the pyridine moiety in the coordination sphere cannot be excluded based on the hyperchromic effect experienced by the electronic $\pi \rightarrow \pi^*$ transition as soon as the metal solution is added to the macrobicycle.

Synthesis and FTIR Spectroscopy of $[Cu(L^1)](ClO_4)_2$. Recrystallization of $[Cu(\mathbf{L^1}H_{-1})]ClO_4 \cdot H_2O$ in a perchloric acid solution afforded dark violet needles which were not suitable for a X-ray diffraction experiment. Thus, structural evidence for the formation of a new species in strongly acid conditions relies essentially on FTIR spectroscopy. Overall, the spectrum looks very similar to that of the starting compound in the 4000−400 cm^{-1} range, although modifications in the carbonyl stretching region support a change in the coordination environment. While the amide I ($\nu_{C=O}$ = 1658 cm^{-1}) and amide II bands (δ_{CNH} = 1531 cm^{-1}) assigned to the unbound peptide group remain unaffected, the $\nu_{C=O}$ mode at 1581 cm^{-1} attributed to the coordinated carboxamide function of $[Cu(\mathbf{L^1}H_{-1})]ClO_4 \cdot H_2O$ is replaced in the acidic form by a strong absorption at 1693 cm^{-1}. This large frequency increase is fully consistent with protonation of the amidato oxygen atom (Cu−N−C═O) to form the iminol tautomer Cu−N═C−OH. Coordinated peptidic nitrogen atoms are expected to become less basic than the carbonyl oxygen center since protonation of the former would annihilate the resonance stabilization energy. Structurally, conversion of an amidato group to the iminol form increases the double-bond character of the C−N bond at the expense of the C═O bond and therefore should result in a shortening of the former and a concomitant lengthening of the latter.

The proposed assignment of the 1693 cm^{-1} band to an iminol $\nu_{C=N}$ vibration is in line with the findings reported by Siegfried et al. for the copper(II) complex of 1,4,8,11-tetraazacyclotetradecane-5-one.[37] Upon protonation of the carbonyl oxygen atom belonging to the nitrogen-bound amide group, the carbon−oxygen distance undergoes a 0.04 Å lengthening while the C−N bond is concomitantly shortened by 0.026 Å. The infrared data obtained for both the unprotonated ($\nu_{C=O}$ = 1562 cm^{-1}) and O-protonated complexes ($\nu_{C=N}$ = 1688 cm^{-1}) are fully consistent with the enolic tautomer structure of the latter species derived by X-ray crystallography. A survey of the Cambridge Structural Database[50−52] revealed two other examples of cyclam-based complexes for which the central metal atom, copper(II) in both cases, is ligated to an iminol moiety.[53,54] Although no structural information is available for the corresponding unprotonated forms preventing a direct comparison of bond distances, infrared absorption features occurring in the 1670−1683 cm^{-1} region were unambiguously attributed to the iminol $\nu_{C=N}$ mode.

Synthesis and FTIR Spectroscopy of $[Cu(\mathbf{L^1}H_{-2})]\cdot 4H_2O$. A different copper(II) complex of cyan-blue color forms when the metalation reaction is carried out in the presence of a weak base like sodium carbonate. Alternatively, the red complex can also be converted into the blue one by increasing the pH of the solution with a mineral base (vide infra). The chemical composition determined by elemental analysis and MALDI-TOF mass spectrometry of the crystals obtained by slow evaporation of an acetonitrile solution is compatible with a $[Cu(\mathbf{L^1}H_{-2})]\cdot 4H_2O$ global formula. The presence of a single $\nu_{C=O}$ stretching band centered at 1555 cm^{-1} in the infrared spectrum supports the abstraction of both amide protons by the added base, thus enabling the coordination of both carboxamido nitrogen atoms to the copper center. Two broad bands at 3430 and 3250 cm^{-1} indicate the presence of hydrogen-bonded water molecules. Since the $\nu_{C=O}$ absorption is shifted to higher energies (1572 cm^{-1}) after partial desiccation of the blue crystals over P_2O_5 under vacuum, it might be inferred that some water molecules interact with the amide groups. Heating leads also to a color change from blue to dark green, implying that the loss of

(42) Bellamy, L. J. *The Infrared Spectra of Complex Molecules*, 3rd ed.; Chapman and Hall: London, 1975; Vol. 1.
(43) Bellamy, L. J. *The Infrared Spectra of Complex Molecules. Advances in Infrared Group Frequencies*, 2nd ed.; Chapman and Hall: London, 1980; Vol. 2.
(44) Silverstein, R. M.; Bassler, G. C.; Morrill, T. C. *Spectrometric Identification of Organic Compounds*, 5th ed.; John Wiley and Sons: New York, 1991.
(45) Kim, M. K.; Martell, A. E. *Biochemistry* **1964**, *3*, 1170.
(46) Kim, M. K.; Martell, A. E. *J. Am. Chem. Soc.* **1966**, *88*, 914.
(47) Pagenkopf, G. K.; Margerum, D. W. *J. Am. Chem. Soc.* **1968**, *90*, 6963.
(48) Brunetti, A. P.; Lim, M. C.; Nancollas, G. H. *J. Am. Chem. Soc.* **1968**, *90*, 5120.
(49) Martell, A. E.; Kim, M. K. *J. Coord. Chem.* **1974**, *4*, 9.
(50) *The Cambridge Structural Database*, release 5.24; Cambridge Structural Database: Cambridge, U.K., 2002.
(51) Allen, F. H. *Acta Crystallogr., Sect. B* **2002**, *58*, 380.
(52) Allen, F. H.; Motherwell, W. D. S. *Acta Crystallogr., Sect. B* **2002**, *58*, 407.
(53) Beveridge, K. A.; McAuley, A.; Xu, C. *Inorg. Chem.* **1991**, *30*, 2074.
(54) Zhu, S.; Kou, F.; Lin, C.; Lin, M.; Chen, Y. *Inorg. Chem.* **1996**, *35*, 5851.

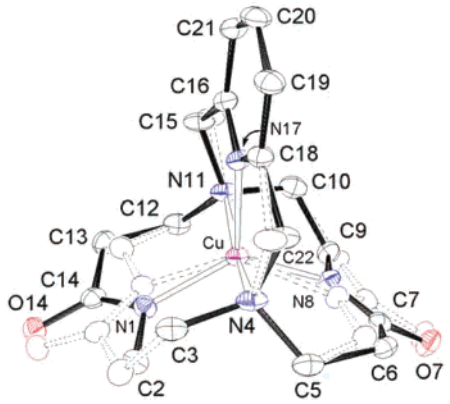

Figure 3. ORTEP view of the structure of [Cu($\mathbf{L^1}H_{-2}$)]·4H_2O showing the atom-labeling scheme and the thermal ellipsoids at the 50% probability level. The minor conformer B found in the unit cell is represented with dashed bonds and nonshaded atoms. All H(−C) hydrogen atoms and the water molecules have been omitted for clarity.

cocrystallized water affects the geometry of the copper chromophore and weakens the ligand-field strength.

Thermal Analysis of [Cu($\mathbf{L^1}H_{-2}$)]·4H_2O. This observation prompted us to undertake a thermogravimetric analysis (TGA) of [Cu($\mathbf{L^1}H_{-2}$)]·4H_2O, coupled with a mass-spectrometric detection of the gases liberated by the sample heated under an oxygen/argon stream. The compound loses 3.65% of its total weight between 45 and 90 °C (T_{onset} = 72 °C), corresponding to the endothermic volatilization of one water molecule/complex (Δm_{calcd} = 3.9%). In the 90−130 °C temperature range, a second weight loss of 7.1% occurs in two overlapping steps and is accompanied by an endothermic DTA signal with a peak temperature T_p equal to 115 °C. The observed mass loss is in good agreement with that calculated for the release of two water molecules/complex (Δm_{calcd} = 8.1%). About 0.5 equiv of water evaporates upon further heating to 230 °C. At this temperature the complex starts to decompose giving rise to a succession of exothermic events with DTA peaks at T_p = 244, 400, and 554 °C, corresponding to the release of water and carbon dioxide.

X-ray Crystal Structure of [Cu($\mathbf{L^1}H_{-2}$)]·4H_2O. Crystallographic and refinement details are listed in Table 1, and selected bond distances and angles are reported in Table 2. The structure revealed a disordered layout of $\mathbf{L^1}$ around the metal center, which affects primarily the 14-membered dioxocyclam moiety. In fact, two conformers with relative site occupation factors of 0.765(4) and 0.235(4), respectively noted A and B, were found to be superimposed. The following pairs of atoms share the same sites: (C3A, C12B); (C3B, C12A); (N4A, N11B); (N4B, N11A); (C5A, C10B); (C5B, C10A). These features allow the pyridine bridge to be connected to the bridgehead nitrogen atoms occupying identical positions in both conformations, avoiding disorder except for the C15 and C22 methylenic carbon atoms. The ORTEP diagram reproduced in Figure 3 highlights the intimate relation between molecules A and B, where each five-membered chelate cycle belonging to the dioxocyclam scaffold of the major species is superimposed with the adjacent six-membered chelate ring of the minor form and vice versa. Thus, isomer B can be approximately described as the mirror image of complex A according to a plane perpendicular to the pyridine ring encompassing the aromatic N17 nitrogen atom and the encapsulated copper center. This close conformational resemblance is clearly evidenced when both structures are overlaid and the deviation between each pair of related non-hydrogen atoms is minimized. A Chem3D least-squares calculation gives a root-mean-square deviation (rmsd) of 0.306 Å for the 25 matched pairs of atoms.

As suggested by FTIR spectroscopy, both carbonyl groups interact via hydrogen bonds with the cocrystallized water molecules, whereas the two amidic nitrogen atoms are deprotonated and bound to the five-coordinate copper(II) cation in agreement with the lengthening of the C7−O7 and the concomitant shortening of the amidato C7−N8 bonds. The structural rearrangement undergone by the macrocyclic cage acting as a pentadentate ligand is reflected by the respective values taken by both folding angles Ω_{13} and Ω_{14} in [Cu($\mathbf{L^1}H_{-2}$)] compared to those of [Cu($\mathbf{L^1}H_{-1}$)]$^+$. Accordingly, the metal lies approximately in the center of the bent 14-membered dioxocyclam ring system (Ω_{14} = 115.8 and 119.5° for molecule A and B, respectively), spanned by the pyridine nucleus (Ω_{13} = 123.4 and 121.6° for molecule A and B, respectively). Hence, $\mathbf{L^1}$ can be considered as a molecular glider, with the complexed copper atom embedded in the center of a cycle composed either of 13 or 14 atoms, depending on the pH at which the metalation reaction has been conducted. Examination of a ball-and-stick molecular model of [Cu($\mathbf{L^1}H_{-1}$)]$^+$ evidenced that a 90° inward rotation of the amidic nitrogen atom brings N8 in an unfavorable binding position for steric reasons. Therefore, the handle containing the amidato group, which is a stronger chelator than the pyridine moiety, flips around the bridgehead tertiary amines by ∼120° to take up the position occupied by the aromatic ring in [Cu($\mathbf{L^1}H_{-1}$)]$^+$.

For the independent [Cu($\mathbf{L^1}H_{-2}$)] molecule labeled A, the Cu−$N_{amidate}$ bond lengths (Cu−N1 = 1.950 Å; Cu−N8 = 1.962(3) Å) are slightly longer than in the tetracoordinated [Cu($\mathbf{L^1}H_{-1}$)]$^+$ cation (Cu−N1 = 1.877(2) Å), as expected on the basis of the ring-size enlargement. Due to a more symmetrical environment provided by the 14-membered cycle in [Cu($\mathbf{L^1}H_{-2}$)], both Cu−N_{amine} distances are also less scattered around their mean (2.026(4) Å) compared to [Cu($\mathbf{L^1}H_{-1}$)]$^+$. The pyridine nitrogen atom is positioned right above the dioxocyclam unit and occupies the apical position, located 1.997(2) Å away from the metal. Thus, the Cu−N17 distance increases by 0.11 Å upon switching from a tetracoordinate to a pentacoordinate metal center. Overall, both [Cu($\mathbf{L^1}H_{-2}$)] isomers found in the crystal structure exhibit virtually the same geometrical parameters although those pertaining to the minor species B are usually less precise. Furthermore, these results are in excellent accordance with the distances reported by Wynn and Hegedus for analogous copper(II) complexes,[30] although the copper−pyridine bond is significantly shorter in the present case (1.997(2) Å compared to 2.12 and 2.13 Å). Examination of the bite-angle values pertaining to isomer A (Table 2) indicates that the coordination polyhedron is best described as a strongly distorted trigonal bipyramid where N1, N8, and N17 define the equatorial plane (average Cu−N_{eq} =

Table 3. UV−Vis and Near-Infrared Spectral Properties of [Cu($\mathbf{L}^1$H$_{-1}$)]ClO$_4$·H$_2$O and [Cu($\mathbf{L}^1$H$_{-2}$)]·4H$_2$O at Room Temperature

	[Cu($\mathbf{L}^1$H$_{-1}$)]ClO$_4$·H$_2$O			[Cu($\mathbf{L}^1$H$_{-2}$)]·4H$_2$O		
assgnt	λ_{max} (nm)		ϵ (M^{-1} cm^{-1})	λ_{max} (nm)		ϵ (M^{-1} cm^{-1})
n, $\pi \rightarrow \pi^*$	208[a]	205[b]	27 000[b]	208[a]	205[b]	25 100[b]
σ(N) → d	270[a]	261[b]	8200[b]	266[a]	260[b]	5820[b]
π(N$^-$) → d	295[a]	297[b]	2430[b]	312[a]	297[b]	2900[b]
d → d	530[a]	520[b]	212[b]	612[a]	600[b]	138[b]
d → d				≈830[a] sh	840[b]	116[b]
d → d				1160[a]	1028[b]	103[b]

[a] Diffuse reflectance data for crystalline material dispersed in barium sulfate. [b] Absorption data for an aqueous solution.

1.97(2) Å), while the N4 and N11 bridgehead amines occupy the axial apexes (average Cu−N$_{ax}$ = 2.026(4) Å). The severe distortion is highlighted by the large deviation experienced by the N4−Cu−N11 (163.8(3)°) and the in-plane trigonal angles (113.1(1), 116.5(1), and 130.4(2)°) from their ideal values of 180 and 120°, respectively. Thus, the angles between adjacent equatorial and axial bonds range from 82.3(1) to 100.1(1)°, the average (89.6°) being close to the ideal value of 90°. The level of angular distortion from both idealized and interconvertible limiting stereochemistries encountered for pentavalent central atoms, namely the regular square-pyramidal (SP) and trigonal bipyramidal (TBP) geometries,[55] is conveniently gauged by the trigonality index τ introduced by Addison et al.[56] According to its definition ($\tau = (\beta - \alpha)/60$, where β is the largest and α the second-largest basal angle), an ideal square-pyramid is characterized by $\tau = 0$, while $\tau = 1$ points out an ideal trigonal bipyramid. The experimental values calculated for both independent [Cu($\mathbf{L}^1$H$_{-2}$)] molecules A and B, respectively 0.557 and 0.473, are in favor of a nearly intermediate structure along the SP-TBP Berry interconversion pathway.[55] Regardless of the limiting geometry considered, the CuN$_5$ polyhedron possesses an approximately C_{2v} symmetry, the 2-fold axis corresponding to the Cu−N17 direction.

UV−Vis Spectroscopy of [Cu($\mathbf{L}^1$H$_{-1}$)]ClO$_4$·H$_2$O and [Cu($\mathbf{L}^1$H$_{-2}$)]·4H$_2$O. Diffuse reflectance spectra of crystalline material finely dispersed in a barium sulfate matrix together with electronic absorption spectra in aqueous solution were recorded to correlate the spectroscopic and structural properties in the solid state and to provide further insights about the geometries adopted by these complexes in solution. Relevant spectroscopic parameters are presented in Table 3. For each compound, the number and shape of the bands together with the corresponding transition energies are virtually identical in both physical states, suggesting that the aforementioned structural features are essentially preserved upon dissolution of the crystals in water.

The UV region is dominated by several, sometimes overlapping, bands associated both to ligand-centered n → π^* ($\lambda_{max} \sim 205-210$ nm; $\epsilon \sim 25\,000$ M^{-1} cm^{-1}) and $\pi \rightarrow \pi^*$ bands (for the free macrocycle the pyridine-centered B band is found at 263.5 nm) and to ligand-to-metal charge transfer (LMCT) transitions. The σ(N) → d excitation of primary and secondary amines coordinated to copper(II) occurs usually around 250−275 nm, whereas further alkylation induces a bathochromic shift.[57] This general trend agrees with the in-plane ligand-field weakening experienced by copper(II) cyclam ($\lambda_{max} = 273$ nm; diffuse reflectance) as the secondary amines are progressively replaced by two ($\lambda_{max} = 283$ nm) and four ($\lambda_{max} = 315$ nm) N-methylated tertiary nitrogen donors. Considering that the ligand-field strength of an amidato anion is stronger than that observed for an amine, the σ(N$^-$) → d LMCT transition is expected to appear at or below 250 nm and should be hypsochromically shifted with respect to the bands originating from the amine nitrogen atoms. In addition, N-bound peptide copper(II) complexes give also rise to intense π(N$^-$) → d transitions near or above 250 nm for square planar geometries.[12,58] Both types of charge-transfer excited states are electric dipole allowed and thus give rise to intense absorption bands.[59] The intensity of the π(N$^-$) → d band is primarily dependent upon the degree of overlap between the π-symmetric orbitals of both the donor and acceptor. Hence, the strong spectral features occurring respectively at ∼260 and ∼300 nm are tentatively ascribed to σ(N) → d and π(N$^-$) → d LMCT bands, in agreement with the characteristic spectroscopic data reported for other transition metal complexes including copper(III) with a donor set consisting of amidato either exclusively or together with amino nitrogen atoms.[60] However, the broadness and lack of well-resolved bands could also suggest that σ and π transitions may overlap. Thus, unambiguous assignment of the experimentally observed UV bands remains a matter of debate.

On the basis of their weak intensity, the low-energy transitions occurring above 400 nm originate from ligand field d → d excitations. To gain further insights into the electronic structure of the copper chromophore, diffuse reflectance and absorption spectra were subjected to Gaussian deconvolution analysis. The individual components shown as dotted lines in Figure 4 were generated with the fitting parameters summarized in Table 4.

Both the solid-state and solution spectra of [Cu($\mathbf{L}^1$H$_{-1}$)]ClO$_4$·H$_2$O display a broad, unsymmetrical band peaking at 520 nm ($\epsilon = 212$ M^{-1} cm^{-1}), which tails off around 800

(55) Kepert, D. L. *Inorganic Stereochemistry*; Springer-Verlag: Heidelberg, Germany, 1982; Vol. 6.
(56) Addison, A. W.; Rao, T. N.; Reedijk, J.; Van Rijn, J.; Verschoor, G. C. *J. Chem. Soc., Dalton Trans.* **1984**, 1349.
(57) Lever, A. B. P. *Inorganic Electronic Spectroscopy*, 2nd ed.; Elsevier: Amsterdam, 1984.
(58) Amundsen, A. R.; Whelan, J.; Bosnich, B. *J. Am. Chem. Soc.* **1977**, *99*, 6730.
(59) Solomon, E. I.; Hare, J. W.; Gray, H. B. *Proc. Natl. Acad. Sci. U.S.A.* **1976**, *73*, 1389.
(60) Lampeka, Y. D.; Gavrish, S. P. *Polyhedron* **2000**, *19*, 2533.

Table 4. Gaussian Analysis of the Room-Temperature Visible and Near-Infrared Ligand-Field Bands of $[Cu(\mathbf{L^1}H_{-1})]ClO_4 \cdot H_2O$ and $[Cu(\mathbf{L^1}H_{-2})] \cdot 4H_2O$

		$[Cu(\mathbf{L^1}H_{-1})]ClO_4 \cdot H_2O$		$[Cu(\mathbf{L^1}H_{-2})] \cdot 4H_2O$	
band	param	reflectance[a]	absorption[b]	reflectance[a]	absorption[b]
1	ν_{max} (cm^{-1})	21 550	21 450	16 398	16 730
	λ_{max} (nm)	464	466	610	598
	$\omega_{1/2}$ (cm^{-1})[c]	2424	2600	3294	3145
	rel area or f[d]	14%	0.001 16[d]	50%	0.002 13[d]
2	ν_{max} (cm^{-1})	19 000	19 160	11 542	12 350
	λ_{max} (nm)	526	522	866	810
	$\omega_{1/2}$ (cm^{-1})[c]	3064	2540	2862	2681
	rel area or f[d]	68%	0.002 13[d]	21%	0.001 35[d]
3	ν_{max} (cm^{-1})	15 950	17 490	8464	9490
	λ_{max} (nm)	627	572	1181	1054
	$\omega_{1/2}$ (cm^{-1})[c]	3093	3610	2369	2749
	rel area or f[d]	18%	0.001 08[d]	29%	0.001 21[d]

[a] Diffuse reflectance data for crystalline material dispersed in barium sulfate. [b] Absorption data for an aqueous solution. [c] Band with at half-maximum. [d] Oscillator strength ($f = 4.315 \times 10^{-9} \int \epsilon \, d\nu$).

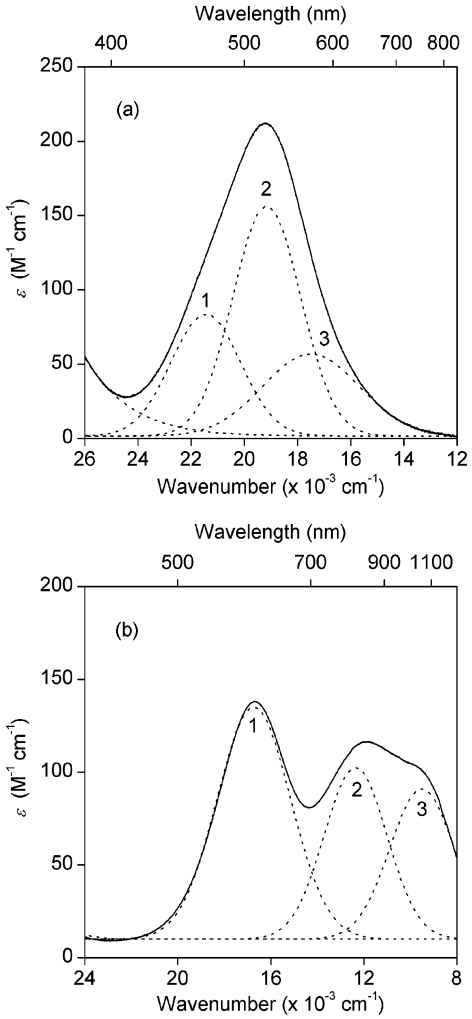

Figure 4. Experimental absorption spectra of (a) $[Cu(\mathbf{L^1}H_{-1})]^+$ and (b) $[Cu(\mathbf{L^1}H_{-2})]$ recorded in the wavenumber scale at a 10 cm^{-1} resolution. Gaussian components are represented as dotted lines. Solvent: H_2O. T = 25 °C.

nm. The position of this maximum falls in the wavelength range commonly observed for square-planar copper(II)−amino acid complexes (480−570 nm)[12,61] and thus reflects a rather strong ligand field at the copper site. The visible absorption profile for $[Cu(\mathbf{L^1}H_{-1})]ClO_4$ could be satisfactorily resolved into three Gaussian peaks centered at 21 450, 19 160, and 17 490 cm^{-1} for the solution spectrum. Very similar results were obtained in the case of the diffuse reflectance powder spectrum, although the low-energy feature occurs at slightly lower energy (15 950 cm^{-1}). Noteworthy, the oscillator strength calculated for the central component ($f = 0.002\,13$) is approximately twice the values found for the lower ($f = 0.001\,08$) and higher energy ($f = 0.001\,16$) bands. In first approximation, the local symmetry of the CuN_4 chromophore can be discussed within the framework of the C_{2v} point group, where the molecular x and y axes are respectively defined as the projections of the $Cu-N_{amidate}$ and $Cu-N_{amine}$ vectors onto the mean CuN_4 plane and the molecular z axis as the normal to both x and y directions. These geometrical constraints imply a $d_{x^2-y^2}$ ground state on the basis of simple symmetry considerations. EPR spectroscopy provided experimental evidence for the ground-state assignment (vide infra). According to the selection rules for electric dipole transitions, four-coordinate tetrahedral-distorted square-planar d^9 complexes give rise to three symmetry-allowed transitions ($d_{xz} \rightarrow d_{x^2-y^2}$, $d_{yz} \rightarrow d_{x^2-y^2}$, and $d_{z^2} \rightarrow d_{x^2-y^2}$ polarized along the x, y, and z axes, respectively). The $d_{xy} \rightarrow d_{x^2-y^2}$ excitation is forbidden in terms of orbital symmetry but can occur by a vibronic mechanism and thus should be less intense compared to the former ones. However, unequivocal assignment of all d−d transitions for approximately square-planar copper(II) complexes is often hampered by the unresolved band shape and also by the difficulty to recognize unambiguously the $d_{z^2} \rightarrow d_{x^2-y^2}$ band. Although tetrahedral distortion weakens significantly the interaction between the $3d_{z^2}$ and 4s orbitals, one should also bear in mind that d−s mixing can be particularly effective and might strongly affect the $d_{z^2} \rightarrow d_{x^2-y^2}$ transition energy.[62]

Moreover, the π-bonding character of both trans-located amidato and pyridine nitrogen donors of $\mathbf{L^1}$ has to be considered.[63,64] Efficient overlap out of the CuN_4 plane of the p_z orbital of these two atoms with the favorably oriented

(61) Prenesti, E.; Daniele, P. G.; Prencipe, M.; Ostacoli, G. *Polyhedron* **1999**, *18*, 3233.
(62) Gerloch, M. *Inorg. Chem.* **1981**, *20*, 638.
(63) Akitsu, T.; Komorita, S.; Urushiyama, A. *Bull. Chem. Soc. Jpn.* **2001**, *74*, 851.
(64) Dudley, R. J.; Hathaway, B. J.; Hodgson, P. G. *J. Chem. Soc., Dalton Trans.* **1972**, 882.

d_{xz} orbital is expected to strongly destabilize it and consequently to lower the $d_{xz} \rightarrow d_{x^2-y^2}$ transition energy. In view of these remarks and despite the difficulty to predict the exact ordering of the spectral terms without any further calculations, the low-energy band at 17 490 cm^{-1} could be reasonably attributed to the allowed $d_{xz} \rightarrow d_{x^2-y^2}$ transition. The 2-fold higher oscillator-strength value (Table 4) found for the component centered at 19 160 cm^{-1} would indicate that the two other *y* and *z*-polarized electronically allowed transitions ($d_{yz} \rightarrow d_{x^2-y^2}$ and $d_{z^2} \rightarrow d_{x^2-y^2}$, respectively) are nearly degenerate, giving rise to a single, twice-intense unresolved band. It follows that the remaining Gaussian peak centered at 21 450 cm^{-1} is tentatively associated with the symmetry-forbidden $d_{xy} \rightarrow d_{x^2-y^2}$ excitation occurring with vibronic intensity only,[64] although the calculated oscillator strength reported in Table 4 seems to be quite high. An alternative interpretation of the electronic absorption properties assumes a C_s stereochemistry of the CuN_4 chromophore, which better reflects the effective molecular symmetry of $[Cu(\mathbf{L^1}H_{-1})]^+$. If we keep the same orientation of the axes, the mirror-symmetry element matches with the (*x*,*z*) plane. Hence, all four transitions become symmetry allowed and thus should occur with similar intensity: d_{xz} (a′) → $d_{x^2-y^2}$ (a′) and d_{z^2} (a′) → $d_{x^2-y^2}$ (a′) being polarized along the *x* and *z* axes, while d_{yz} (a″) → $d_{x^2-y^2}$ (a′) and d_{xy} (a″) → $d_{x^2-y^2}$ (a′) are *y*-polarized.

The visible diffuse reflection spectrum of the microcrystalline $[Cu(\mathbf{L^1}H_{-2})]\cdot 4H_2O$ blue complex, which displays a broad manifold with two peaks at 612 and 1160 nm with a shoulder at ~830 nm, is fully consistent with a CuN_5 chromophore. Band deconvolution revealed three electronic transitions in the 8000−22 000 cm^{-1} region (Table 4). Moreover, the relative intensity of the low- and high-energy bands is diagnostic of the exact nature of the pentacoordinate geometry. For a regular trigonal bipyramidal (TBP) chromophore such as $[Cu(tren)(NH_3)](ClO_4)_2$ (ν_{max} = 11 400 cm^{-1} with a shoulder at 15 200 cm^{-1}),[65] the most intense absorption corresponds to the low energy component. The reverse pattern is normally observed when the environment around the copper cation is square-pyramidal,[66−71] as found for $K[Cu(NH_3)_5](PF_6)_3$ (ν_{max} = 15 300 cm^{-1} with a shoulder at 11 400 cm^{-1}).[65] In comparison, the transition for $[Cu(\mathbf{L^1}H_{-2})]\cdot 4H_2O$ occurs at higher energy, indicating a stronger ligand-field strength. Upon heating of the hydrated species under vacuum, all three Gaussian lines initially centered at 16 398, 11 542, and 8464 cm^{-1} are shifted to lower energies by 260, 680, and 464 cm^{-1}, respectively, in line with the observed color change from blue to green. Thus, the breaking of the C═O···H_2O hydrogen bonds due to the concomitant water loss weakens the ligand-field strength of $\mathbf{L^1}$.

The absorption spectrum of an aqueous $[Cu(\mathbf{L^1}H_{-2})]$ solution exhibits two bands with similar absorptivities at 600 nm (ϵ = 138 M^{-1} cm^{-1}) and 840 nm (ϵ = 116 M^{-1} cm^{-1}), which is accompanied by a low-energy shoulder (λ_{max} = 1028 nm; ϵ = 103 M^{-1} cm^{-1}) extending up to 1500 nm. The close resemblance of the Gaussian band-shape parameters for the powder and solution spectra (Table 4) further supports the idea that the complex undergoes only very limited conformational rearrangements upon dissolution in a strongly solvating medium. Since the oscillator strength found for the high-energy component (ν_{max} = 16 730 cm^{-1}; f = 0.002 13) is very close to the sum found for the two other bands (Σf = 0.002 56), an intermediate stereochemistry between a square-planar pyramid and a trigonal bipyramid is inferred,[72] in agreement with the distorted coordination polyhedron evidenced by the crystal structure analysis. However, the bathochromic shift experienced by all three Gaussian bands relative to the solid-state spectrum suggests that the complex adopts a geometry closer to the trigonal bipyramid in solution.[71] The typical "inverted axial" appearance of the EPR spectrum of a frozen sample further supports the TBP geometry associated with a d_{z^2} ($^2A_1'$) ground state (vide infra).

The three component ligand-field spectrum is best interpreted using the C_{2v} selection rules, because only two transitions are expected in D_{3h} symmetry and spin−orbit coupling cannot account for the observed band separation. Indeed, this effect would only split the E′ state to the maximum extent of 1658 cm^{-1}, corresponding to twice the value of the Landé factor, assuming that the orbital reduction factor *k* equals 1.[73] When the symmetry is lowered from D_{3h} to C_{2v} with the *x* axis oriented along the $Cu-N_{pyridine}$ vector and the *z* direction taken as the principal axis (i.e. along the $N_{amine}-Cu-N_{amine}$ direction), the degeneracy of the $^2E''$ and $^2E'$ excited states is lifted: the E′ level splits into $^2A_1$ ($d_{x^2-y^2}$) and $^2B_1$ (d_{xy}), while the E″ term leads to $^2B_2$ (d_{xz}) and $^2A_2$ (d_{yz}) states. The representation of the five σ orbitals reduces to $3A_1 + B_1 + B_2$; hence, solely the d_{yz} orbital is nonbonding and is therefore assumed as the most stable in energy. Symmetry and overlap arguments lead us to propose the following order of levels: $^2A_2$ (d_{yz}) > $^2B_2$ (d_{xz}) > $^2B_1$ (d_{xy}) > $^2A_1$ ($d_{x^2-y^2}$) > $^2A_1$ (d_{z^2}).[74] Moreover, π interactions involving the equatorial set of amidato and pyridine nitrogen donors require d orbitals having either a_1 or b_1 and b_1 symmetry, respectively, therefore contributing to destabilize the $^2B_1$ (d_{xy}), $^2A_1$ ($d_{x^2-y^2}$), and $^2A_1$ (d_{z^2}) states. Among the four possible transitions, only the $d_{yz} \rightarrow d_{z^2}$ ($^2A_1 \rightarrow {}^2A_2$) is forbidden in all polarizations by a static electric dipole mechanism, but it may occur with low intensity via vibronic coupling.[75] On the basis of these general considerations, the Gaussian peaks centered at 9490 and 12 350 cm^{-1} are

(65) Duggan, M.; Ray, N.; Hathaway, B. J.; Tomlinson, G.; Brint, P.; Pelin, K. *J. Chem. Soc., Dalton Trans.* **1980**, 1342.
(66) Addison, A. W.; Hendriks, H. M. J.; Reedijk, J.; Thompson, L. K. *Inorg. Chem.* **1981**, *20*, 103.
(67) Harrison, W. D.; Kennedy, D. M.; Power, M.; Sheahan, R.; Hathaway, B. J. *J. Chem. Soc., Dalton Trans.* **1981**, 1556.
(68) Tyagi, S.; Hathaway, B. J. *J. Chem. Soc., Dalton Trans.* **1981**, 2029.
(69) Hathaway, B. J. In *Comprehensive Coordination Chemistry*; Wilkinson, G., Gillard, R. D., McCleverty, J. A., Eds.; Pergamon Press: Oxford, U.K., 1987; Vol. 5, p 533.
(70) Wei, N.; Murthy, N. N.; Karlin, K. D. *Inorg. Chem.* **1994**, *33*, 6093.
(71) McLachlan, G. A.; Fallon, G. D.; Martin, R. L.; Spiccia, L. *Inorg. Chem.* **1995**, *34*, 254.
(72) Schatz, M.; Becker, M.; Thaler, F.; Hampel, F.; Schindler, S.; Jacobson, R. R.; Tyeklar, Z.; Murthy, N. N.; Ghosh, P.; Chen, Q.; Zubieta, J.; Karlin, K. D. *Inorg. Chem.* **2001**, *40*, 2312.
(73) Slade, R. C.; Tomlinson, A. A. G.; Hathaway, B. J.; Billing, D. E. *J. Chem. Soc. A* **1968**, 61.
(74) Reinen, D.; Atanasov, M. *Chem. Phys.* **1989**, *136*, 27.

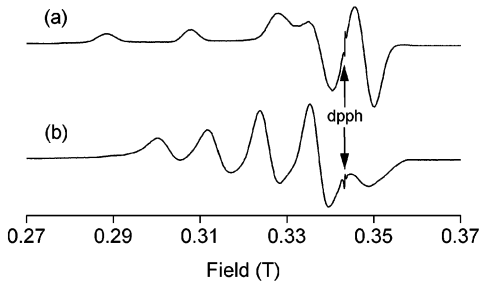

Figure 5. X-band EPR spectra of (a) $[Cu(\mathbf{L^1}H_{-1})]ClO_4 \cdot H_2O$ and (b) $[Cu(\mathbf{L^1}H_{-2})] \cdot 4H_2O$ in frozen water/ethylene glycol mixture (7/3 v/v): $T =$ 100 K; modulation frequency, 100 kHz; modulation amplitude, 1 mT; microwave power, 63 mW; $g_{dpph} = 2.0036$.

respectively assigned to the $^2A_1$ ($d_{x^2-y^2} \rightarrow d_{z^2}$) and $^2B_1$ ($d_{xy} \rightarrow d_{z^2}$) components of the split E′ term, in agreement with literature data.[76,77] The similar oscillator-strength values found for these *x*- and *y*-polarized transitions further support the attribution. Consequently, the remaining and most intense band at 16 730 cm^{-1} arises from the symmetry-allowed $d_{xz} \rightarrow d_{z^2}$ excitation having *z* polarization. The higher oscillator strength associated with that component (Table 4) suggests that the $d_{yz} \rightarrow d_{z^2}$ transition, only allowed through vibronic coupling, is most probably overlapping. This assumption is supported by angular overlap model (AOM) calculations carried out for a C_{2v}-symmetric chromophore by several groups in an attempt to correlate on a more quantitative basis the energy variations of the d orbitals with the degree of distortion.[74,76,78−80] These authors were able to predict that deviation from the ideal D_{3h} symmetry would create only a small energy gap between both $^2B_2$ (d_{xz}) and $^2A_2$ (d_{yz}) levels originating from the E″ state.

EPR Spectroscopy of $[Cu(\mathbf{L^1}H_{-1})]ClO_4 \cdot H_2O$ and $[Cu(\mathbf{L^1}H_{-2})] \cdot 4H_2O$. Room-temperature and frozen-solution (100 K) X-band EPR spectra were recorded in a binary water/ethylene glycol mixture (7/3 v/v). This medium was preferred over pure water because it gives a glass of higher quality compared to ice. At low temperature, each complex displays an anisotropic $S = {}^1/_2$ signal at $g \sim 2$ (Figure 5), suggesting an axial symmetry in first approximation. In the liquid state, typical isotropic spectra were obtained with four equally spaced absorptions due to the coupling of the unpaired electron with the $I = {}^3/_2$ nuclear spin on both ^{63}Cu and ^{65}Cu isotopes.

The anisotropic spectral morphology ($g_{\parallel} > g_{\perp} > g_e =$ 2.0023) found for the tetracoordinate $[Cu(\mathbf{L^1}H_{-1})]^+$ species is typical of a tetragonally distorted CuN_4 stereochemistry assuming a $d_{x^2-y^2}$ ground state, in agreement with the structural and electronic absorption data. Hyperfine splitting is well-resolved only in the parallel region. The spin-Hamiltonian parameters deduced from the high- ($g_{iso} = 2.08$, $A_{iso} = 77 \times 10^{-4}$ cm^{-1}) and low-temperature spectra ($g_{\parallel} =$ 2.17, $g_{\perp} = 2.04$, $A_{\parallel} = 192 \times 10^{-4}$ cm^{-1}, $A_{\perp} = 19 \times 10^{-4}$ cm^{-1}) are close to those determined for the related tetracoordinated copper complexes of $\mathbf{L^2}$ and $\mathbf{L^3}$ [19] and fall in the typical range reported for 5,7-dioxocyclam and other amidato-based ligands.[54,81−83] However, the deviation experienced by the CuN_4 chromophore of $[Cu(\mathbf{L^1}H_{-1})]$ from a square-planar arrangement as found for $[Cu(\mathbf{L^3}H_{-2})]$ is evidenced by the relatively higher value taken by the $g_{\parallel}/A_{\parallel}$ ratio (113 vs 105 cm, respectively). Larger $A_{\parallel}$ values are consistent with stronger in-plane ligand-field strength due to a more efficient overlap between the metal ($d_{x^2-y^2}$) and donor-atom centered orbitals.

In contrast, the frozen-state spectrum of the five-coordinate $[Cu(\mathbf{L^1}H_{-2})]$ compound is composed of a very intense perpendicular signal at $g_{\perp} = 2.15$ with a clear resolution of the four copper hyperfine lines ($|A_{\perp}| = 116 \times 10^{-4}$ cm^{-1}). The parallel contribution appears much less intense and displays no apparent hyperfine splitting. An approximate value of $g_{\parallel} = 2.04$ was estimated from the isotropic spin-Hamiltonian factors obtained at room temperature: $g_{iso} =$ 2.112; $A_{iso} = 67 \times 10^{-4}$ cm^{-1}. The "inverted axial" pattern ($g_{\perp} > g_{\parallel} \sim g_e$) is indicative of a trigonal electronic ground state (i.e. d_{z^2}), in accordance with a TBP-like arrangement of the nitrogen donor atoms. In the simplest approximation where the ligand does not contribute to the orbital angular momentum, the $g_{\parallel}$ value should equal g_e (2.0023) for a D_{3h} symmetry. In practice, slightly lower $g_{\parallel}$ values might be expected because of the inclusion of quadratic terms containing the spin−orbit coupling constant in the expression of the tensor.[65,84] In turn, temperature-dependent positive deviations from the theoretical g_e value have been justified by invoking a vibronic coupling that allows the mixing of different excited states into the ground level.[85] Considering the intermediate geometry of $[Cu(\mathbf{L^1}H_{-2})]$, strong rhombic distortions might be expected, which should mainly affect the g_y and A_y factors.[79]

Solution Equilibrium Studies of the Copper(II) Complexes. Cyclic *cis*- and *trans*-dioxotetraamines are well-known to form moderately stable copper(II) complexes in aqueous solution. The metal-assisted deprotonation of the amide nitrogen atom of 5,12-dioxocyclam ($\mathbf{L^2}$) or its 1,8-dimethyl derivative ($\mathbf{L^3}$) occurs typically at pH values above ~4, the $[Cu(\mathbf{L}H_{-2})]$ complexes being totally dissociated under more acidic conditions.[19] In comparison, the macrobicyclic species $[Cu(\mathbf{L^1}H_{-1})]^+$ exhibits a remarkable inert character with respect to the proton-assisted dissociation even in highly concentrated acid solutions, since any significant dissociation could be detected. Owing to the infrared analysis of the violet material isolated from a perchloric acid solution,

(75) Procter, I. M.; Hathaway, B. J.; Billing, D. E.; Dudley, R.; Nicholls, P. *J. Chem. Soc. A* **1969**, 1192.
(76) Bencini, A.; Gatteschi, D. *Inorg. Chem.* **1977**, *16*, 1994.
(77) Murakami, T.; Takei, T.; Ishikawa, Y. *Polyhedron* **1997**, *16*, 89.
(78) Hitchman, M. A. *Inorg. Chem.* **1974**, *13*, 2218.
(79) Bencini, A.; Bertini, I.; Gatteschi, D.; Scozzafava, A. *Inorg. Chem.* **1978**, *17*, 3194.
(80) Reinen, D.; Friebel, C. *Inorg. Chem.* **1984**, *23*, 791.
(81) Kimura, E.; Shionoya, M.; Okamoto, M.; Nada, H. *J. Am. Chem. Soc.* **1988**, *110*, 3679.
(82) Luo, Q. H.; Zhu, S. R.; Shen, M. C.; Yu, S. Y.; Zhang, Z.; Huang, X. Y.; Wu, Q. J. *J. Chem. Soc., Dalton Trans.* **1994**, 1873.
(83) Santos, M. A.; Gaspar, M.; Amorim, M. T. *Inorg. Chim. Acta* **1999**, *284*, 20.
(84) Barbucci, R.; Bencini, A.; Gatteschi, D. *Inorg. Chem.* **1977**, *16*, 2117.
(85) Bencini, A.; Gatteschi, D. In *Transition Metal Chemistry, A Series Of Advances*; Melson, G. A., Figgis, B. N., Eds.; Marcel Dekker: New York, 1965; Vol. 8, p 1.

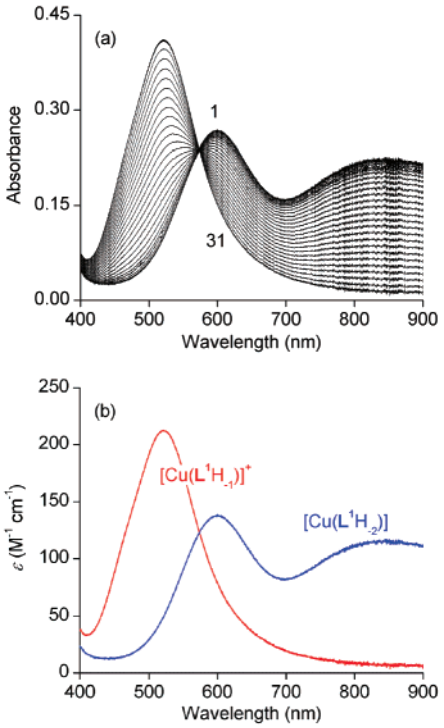

Figure 6. (a) Spectrophotometric titration of a 2 mM [Cu($\mathbf{L^1}H_{-2}$)] solution by a standardized 0.1 M HNO_3 solution. $I = 0.1$ M KNO_3, $T = 25$ °C, and $l = 1$ cm. Spectra 1−31: p[H] = 11.04, 10.94, 10.80, 10.62, 10.31, 10.06, 9.90, 9.74, 9.56, 9.45, 9.32, 9.21, 9.10, 9.00, 8.91, 8.83, 8.74, 8.65, 8.56, 8.47, 8.36, 8.26, 8.13, 7.97, 7.76, 7.42, 6.41, 4.36, 3.86, 3.64, 3.39. (b) Calculated electronic spectra (bottom) of both [Cu($\mathbf{L^1}H_{-1}$)]$^+$ and [Cu($\mathbf{L^1}H_{-2}$)] species.

the hypsochromic shift of the metal-centered absorption band in the electronic spectrum is assigned to the formation of the iminol complex. Since only very limited spectral changes could be observed in moderately acidic aqueous solutions (pH ∼ 2), no further attempts were made to study quantitatively the protonation equilibrium.

The pH-triggered interconversion of the red, tetracoordinated complex into the blue, pentacoordinated [Cu($\mathbf{L^1}H_{-2}$)] neutral species provides a unique example of a pH-induced metal-ion translocation,[86,87] where the molecular reorganization could be easily monitored by visible absorption spectroscopy in the 400−900 nm range upon titrating a 2 mM aqueous solution of [Cu($\mathbf{L^1}H_{-1}$)]$^+$ with a standardized 0.1 M KOH solution. The reversibility of the reaction was clearly established by a back-titration from high down to low pH using a standardized 0.1 M HNO_3 solution. Identical results were further obtained by a direct acidimetric titration, starting with an alkaline solution obtained by dissolving crystals of [Cu($\mathbf{L^1}H_{-2}$)]·$4H_2O$. A typical set of absorption spectra, recorded at 25 °C in 0.1 M KNO_3 for p[H] values (p[H] = −log [H_3O^+]) in the 3.39−11.04 range, is reproduced in Figure 6.

The occurrence of an isosbestic point at 574 nm as well as a factor analysis of the entire data set suggests that only two absorbing species, corresponding to both forms of the copper(II) complex, are in equilibrium. Simultaneous refinements of the potentiometric and spectrophotometric data by both nonlinear least squares programs HYPERQUAD 2000[88] and SPECFIT[89−91] confirmed that only 1 equiv of acid/molecule of [Cu($\mathbf{L^1}H_{-1}$)]$^+$ is required to protonate and decoordinate one amidato group. The pK_a value associated with equilibrium (1), averaged out of three separate titrations, was found to be equal to 8.73(2). The calculated electronic absorption spectra of both complexes shown in the bottom part of Figure 6 are in excellent agreement with those recorded directly from pure samples.

$$[\mathrm{Cu}(\mathbf{L^1}H_{-1})]^+ \overset{pK_a}{\rightleftharpoons} [\mathrm{Cu}(\mathbf{L^1}H_{-2})] + H^+ \qquad (1)$$

The amide proton abstraction from the tetracoordinated [Cu($\mathbf{L^1}H_{-1}$)]$^+$ species, which is followed by a conformational rearrangement, is fully reversible with respect to pH and moreover is a fast process. Indeed, in an attempt to study the interconversion kinetics using a stopped-flow instrument, the reaction already reached completion during the mixing time estimated to be in the order of 1.5 ms. Likewise, the proton-driven translocation of the central Cu^{2+} ion in a ditopic phenanthrolinophane ligand from the α,α′-diimine to the polyamine unit was found to occur in the submillisecond time scale, whereas the reverse motion required less than 1 s.[87]

Interestingly, the measured pK_a value of 8.73 parallels the ionization constants reported in the literature for a series of ternary [Cu(bipy)L]$^{2+}$ complexes formed between copper(II), 2,2′-bipyridine (bipy), and various glycyl peptides (L).[12] A square-planar structure has been suggested for these complexes, involving the heteroaromatic bischelate ligand, the amino group, and the carbonyl oxygen atom. The pK_a values corresponding to the deprotonation of the amide nitrogen atom were found to be quite similar for L = glycinamide (7.71), glycylglycinate (7.77), glycylglycylamide (∼7.4), triglycinate (8.17), or tetraglycinate (∼8.5), suggesting a common coordination scheme for all these [Cu(bipy)(LH_{-1})]$^+$ species where the amidic oxygen has been replaced by the ionized amidato nitrogen atom.[12] Although the situation is somewhat different in the case of [Cu($\mathbf{L^1}H_{-1}$)]$^+$ since none of the carbonyl oxygen atoms interact with the metal, one might conclude that the precise nature of the residue containing the peptide bond lacks influence on the acidity constant, provided the chain is flexible enough to allow the binding of the amidato nitrogen atom. The free-energy gain associated to the expansion of the approximately square-planar coordination sphere toward a distorted trigonal bipyramid may provide the necessary driving force promoting the deprotonation of the free amide moiety under weakly

(86) Anda, C.; Bazzicalupi, C.; Bencini, A.; Bianchi, A.; Fornasari, P.; Giorgi, C.; Valtancoli, B.; Lodeiro, C.; Parola, A. J.; Pina, F. *Dalton Trans.* **2003**, 1299.
(87) Mendoza, A.; Aguilar, J.; Basallote, M. G.; Gil, L.; Hernandez, J. C.; Manez, M. A.; Garcia-Espana, E.; Ruiz-Ramírez, L.; Soriano, C.; Verdejo, B. *Chem. Commun.* **2003**, 3032.
(88) Gans, P.; Sabatini, A.; Vacca, A. *Talanta* **1996**, *43*, 1739.
(89) Gampp, H.; Maeder, M.; Meyer, C. J.; Zuberbühler, A. D. *Talanta* **1985**, *32*, 95.
(90) Gampp, H.; Maeder, M.; Meyer, C. J.; Zuberbühler, A. D. *Talanta* **1985**, *32*, 251.
(91) Gampp, H.; Maeder, M.; Meyer, C. J.; Zuberbühler, A. D. *Talanta* **1985**, *32*, 1133.

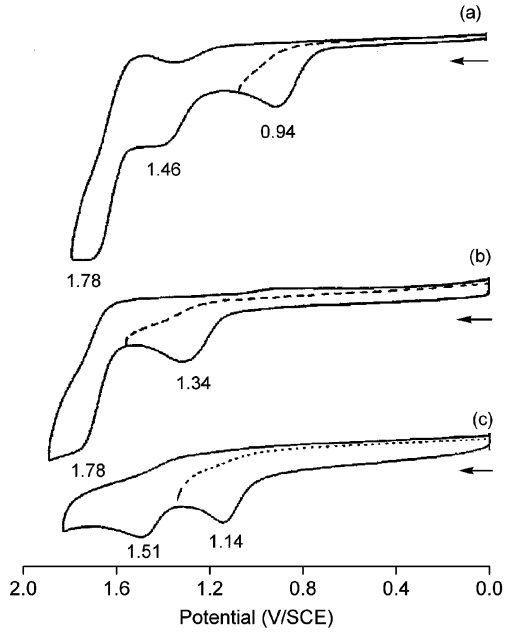

Figure 7. Cyclic voltammograms for the oxidation under N_2 of (a) $[Cu(\mathbf{L^1}H_{-2})]\cdot 4H_2O$, (b) $[(Cu(\mathbf{L^1}H_{-1})]ClO_4\cdot H_2O$, and (c) $\mathbf{L^1}$: solvent, CH_3CN; $I = 0.1$ M $[N(n\text{-}C_4H_9)_4]ClO_4$; $\upsilon = 100$ mV s^{-1}; working electrode, glassy carbon.

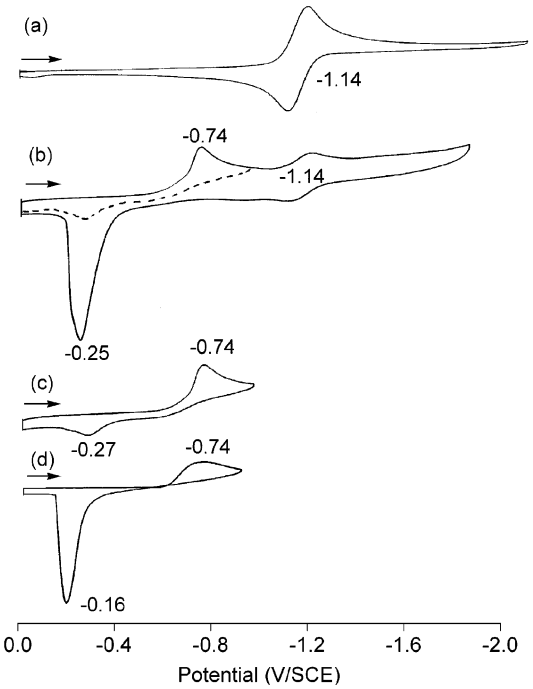

Figure 8. Cyclic voltammograms for the reduction under N_2 of (a) $[Cu(\mathbf{L^1}H_{-2})]\cdot 4H_2O$, (b) $[Cu(\mathbf{L^1}H_{-1})]ClO_4\cdot H_2O$, (c) $[Cu(\mathbf{L^1}H_{-1})]ClO_4\cdot H_2O$ reverse after first reduction, and (d) $[Cu(CH_3CN)_4]PF_6$: solvent, CH_3CN; $I = 0.1$ M $[N(n\text{-}C_4H_9)_4]ClO_4$; $\upsilon = 100$ mV s^{-1}; working electrode: glassy carbon.

basic conditions and its subsequent binding to the copper center, thus rotating the pyridine ring out of the mean donor plane.

Electrochemistry and UV−Vis Spectroelectrochemistry of $[Cu(\mathbf{L^1}H_{-1})]ClO_4\cdot H_2O$ and $[Cu(\mathbf{L^1}H_{-2})]\cdot 4H_2O$. The electrochemical properties of both copper complexes were investigated by cyclic voltammetry at a glassy-carbon working electrode. All experiments were carried out in acetonitrile solutions containing 0.1 M $[N(n\text{-}C_4H_9)_4]ClO_4$ as supporting electrolyte.

In the anodic region, the cyclic voltammogram of $[Cu(\mathbf{L^1}H_{-2})]\cdot 4H_2O$ (Figure 7a) shows three irreversible peaks at $E_p = 0.94$, 1.46, and 1.78 V/SCE ($\upsilon = 100$ mV s^{-1}), while $[Cu(\mathbf{L^1}H_{-1})]ClO_4\cdot H_2O$ undergoes two irreversible processes at $E_p = 1.34$ and 1.78 V/SCE under the same experimental conditions (Figure 7b). Moreover, the electrochemical behavior of both complexes is also quite similar to that displayed by the free-base ligand $\mathbf{L^1}$ ($E_p = 1.14$ and 1.51 V/ECS; Figure 7c), suggesting ligand-centered oxidation processes and coupled chemical reactions which lead to the irreversibility. The assumption of ligand-centered rather than metal-centered oxidation was corroborated by spectroelectrochemical UV−vis data obtained in a thin-layer cell (OTTLE). Indeed, the ligand-field transitions characteristic of a d^9 electronic configuration of the copper center are not perturbed, whereas the LMCT band centered at 348 nm undergoes a slight hypochromic effect during the electrolysis.

The reductions of both compounds were also investigated in acetonitrile under an inert atmosphere (N_2). The pentacoordinate complex $[Cu(\mathbf{L^1}H_{-2})]\cdot 4H_2O$ undergoes a reversible ($\Delta E = 80$ mV at $\upsilon = 25$ mV s^{-1}) to quasi-reversible reduction ($\Delta E = 220$ mV at $\upsilon = 500$ mV s^{-1}) at $E_{1/2} = -1.14$ V/SCE (Figure 8a), and this is attributed to a single electron transfer from the Cu(II) to the Cu(I) complex on the basis of in situ UV−vis spectroelectrochemical data. Figure 9a depicts the spectral changes which occur between 300 and 900 nm during controlled-potential reduction of $[Cu(\mathbf{L^1}H_{-2})]$ at −1.40 V/SCE. The d → d transition initially centered at 611 nm progressively disappears, while the intensity of the 348 nm feature ascribed to a LMCT band is considerably weakened as the reduction of the copper(II) center proceeds to completion, giving rise to three well-defined isosbestic points. The copper(I) reduction product is assigned as the $[Cu(\mathbf{L^1}H_{-2})]^-$ species, which is chemically stable by virtue of the well-defined cyclic voltammogram displayed in Figure 8a.

This reduction behavior contrasts that of $[Cu(\mathbf{L^1}H_{-1})]ClO_4\cdot H_2O$ at a scan rate of 100 mV s^{-1} (Figure 8b). An irreversible peak is seen at $E_p = -0.74$ V/SCE, which splits into two components ($E_p = -0.70$ and −0.80 V/SCE) upon increasing the scan rate to 500 mV s^{-1} (Figure S1, Supporting Information). There is also a reoxidation peak ($E_p = -0.25$ V/SCE) on the reverse scan, which is indicative of a Cu(0) to Cu(I) surface reaction. The formation of a copper layer on a platinum electrode surface polarized for ca. 2 min at a potential of −0.90 V/SCE was visually observed, and it is therefore concluded that the oxidation peak at $E_p = -0.25$ V/SCE is related to copper(0) dissolution. As seen in Figure 8b, extending the initial reductive potential sweep to −1.8 V/SCE leads to a second quasi-reversible reduction centered at $E_{1/2} = -1.14$ V/SCE (Figure 8b). Noteworthy, the half-wave potential for this redox process is located at exactly the same position as for $[Cu(\mathbf{L^1}H_{-2})]$, suggesting that both processes are due to reduction and reoxidation of the same species. This assumption was further supported by the changes in relative intensity of the current for both peaks of

Scheme 1

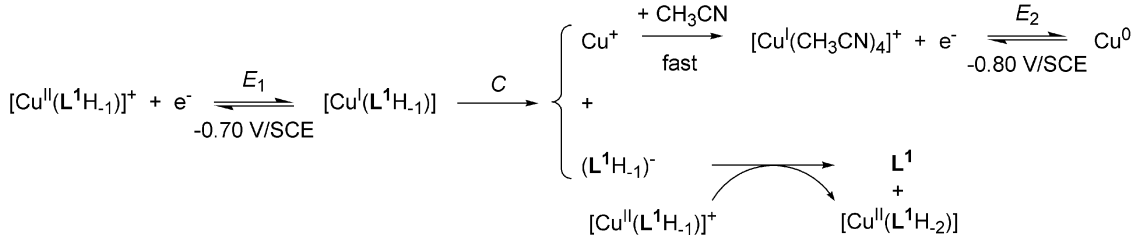

$[Cu(\mathbf{L^1}H_{-1})]^+$ as the scan rate was varied. The most cathodic signal in Figure 8b tended to vanish at slower scan rates ($v < 10$ mV s^{-1}) indicating that the reduced species had enough time to diffuse away from the electrode, but it approached a limiting 2:1 intensity ratio at higher sweep rates (Figure S1, Supporting Information).

Further insights regarding the product(s) formed during the reduction of an acetonitrile solution containing the red $[Cu(\mathbf{L^1}H_{-1})]ClO_4 \cdot H_2O$ compound are given by the UV−vis changes which occur in the spectroelectrochemical cell during controlled-potential reduction at −0.9 V/SCE. The spectroscopic data reproduced in Figure 9b document the progressive appearance of two new absorptions at 348 and 611 nm, which correspond to the marker bands of the blue $[Cu(\mathbf{L^1}H_{-2})]$ species. Spectral changes corresponding to the second reduction of $[Cu(\mathbf{L^1}H_{-1})]^+$ were also recorded at a potential of −1.40 V/SCE and were similar to those obtained for the first reduction process ($E_{app} = -0.9$ V/SCE). Most interestingly, these changes were also identical with those recorded for the genuine $[Cu(\mathbf{L^1}H_{-2})]$ complex (Figure 9a). Finally, a differential spectroelectrochemical experiment was carried out at −0.85 V/ SCE in the infrared region and provided evidence for loss of free ligand from reduced $[Cu(\mathbf{L^1}H_{-1})]^+$ in solution along with the concomitant formation of pentacoordinate $[Cu(\mathbf{L^1}H_{-2})]$. Two positive infrared bands appeared at 1686 and 1599 cm^{-1} during reduction in the thin-layer cell, which are attributed to the C═O vibrations of free $\mathbf{L^1}$ and $[Cu(\mathbf{L^1}H_{-2})]$, respectively.

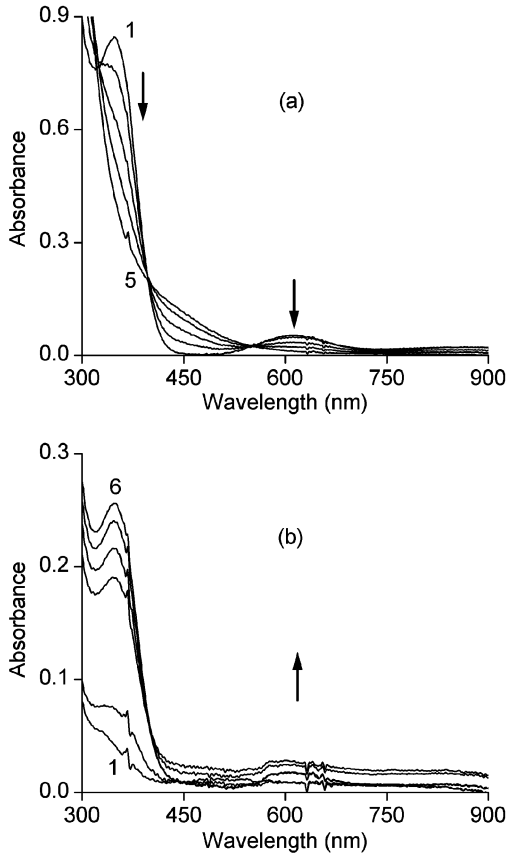

Figure 9. UV−vis spectral changes recorded in the course of the reduction under N_2 for (a) $[Cu(\mathbf{L^1}H_{-2})] \cdot 4H_2O$ at −1.40 V/SCE and (b) $[Cu(\mathbf{L^1}H_{-1})]ClO_4 \cdot H_2O$ at −0.90 V/SCE within a spectroelectrochemical OTTLE cell: solvent, CH_3CN; $I = 0.1$ M $[N(n\text{-}C_4H_9)_4]ClO_4$.

The electrochemical and spectroeletrochemical data are self-consistent and indicate that a stable reaction product generated during the first reduction of the red tetracoordinate $[Cu(\mathbf{L^1}H_{-1})]^+$ complex corresponds to the blue pentacoordinate $[Cu(\mathbf{L^1}H_{-2})]$ species. Since the oxidation state of the copper center is +II for the reactant $[Cu(\mathbf{L^1}H_{-1})]^+$ as well as for the $[Cu(\mathbf{L^1}H_{-2})]$ product, a complex two-electron-transfer mechanism coupled with chemical steps must be invoked to account for the experimental observations.[92,93] The proposed mechanism is shown in Scheme 1.

According to this scheme, the tetracoordinate copper(II) atom of $[Cu(\mathbf{L^1}H_{-1})]^+$ is reduced at $E_p = -0.70$ V/SCE (E_1) giving an unstable copper(I) $[Cu(\mathbf{L^1}H_{-1})]$ intermediate, which dissociates (C) liberating a copper(I) cation and a molecule of ligand possessing one deprotonated amide group. The copper(I) ion is rapidly solvated by acetonitrile to give $[Cu(CH_3CN)_4]^+$, which undergoes reduction to metallic copper (E_2) at the applied potential of −0.70 V/SCE. This assignment is supported by the E_p value of −0.74 V/SCE, which was measured independently for $[Cu(CH_3CN)_4]PF_6$ under identical experimental conditions (Figure 8d). Thus, as a consequence of the redox-induced dissociation of $[Cu(\mathbf{L^1}H_{-1})]^+$ and subsequent release of the anionic $(\mathbf{L^1}H_{-1})^-$ species which can be considered as a very strong organic base in solution, a proton transfer reaction has to occur. Most likely, it involves a weakly acidic (vide supra) yet unreacted $[Cu(\mathbf{L^1}H_{-1})]^+$ entity as proton donor, which is converted into the neutral pentacoordinated copper(II) species by deprotonation and coordination of the unbound amide group. Hence, the second reversible cathodic peak appearing at −1.14 V/SCE (Figure 8b) is attributed to the reduction of $[Cu(\mathbf{L^1}H_{-2})]$ which is formed in the diffusion layer, in full agreement with the UV−vis and IR spectroscopic results. Overall, 2 equiv of $[Cu(\mathbf{L^1}H_{-1})]^+$ are involved in the process, one being reduced at the electrode and the other serving as a proton mediator in the diffusion layer.

(92) Zanello, P.; Cinquantini, A.; Guerriero, P.; Tamburini, S.; Vigato, P. A. *Inorg. Chim. Acta* **1986**, *117*, 91.
(93) Taha, A. *New J. Chem.* **2001**, *25*, 853.

Conclusion

Cross-bridging the 1 and 8 positions of 5,12-dioxocyclam with a 2,6-pyridyl group affords a hemispherical macrobicyclic ligand displaying a split personality. The stepwise deprotonation of the amide groups is promoted by the presence of a copper(II) salt, affording either a tetracoordinate or a pentacoordinate complex depending upon the pH of the reaction mixture. Both species have been characterized by means of X-ray crystallography, spectroscopic, and electrochemical techniques. The inert character of the monoamidate species toward dissociation in strongly acidic conditions is highlighted by its ability to form a monoprotonated iminol complex. In weakly basic solution, the rapid and reversible interconversion of the four-coordinate mono- into the five-coordinate bis(amidate) is pH-triggered and is accompanied by a change in color. The unusual coordination properties exhibited by this *ansa*-dioxocyclam cage are also reflected by peculiar electrochemical characteristics of the corresponding copper complexes. To unravel the influence of the cross-bridging unit, further studies involving analogous ligands that lack a coordinating pyridine group are underway and will be reported in due course.

Experimental Section

Safety Note. *Although no problems were experienced in handling perchlorate compounds, these salts when combined with organic ligands are potentially explosive and should be manipulated with care and used only in small quantities.*

Preparation of Compounds. Unless otherwise noted, all chemicals and starting materials were obtained commercially and used without further purification. Compound **L¹** was synthesized according to a previously published procedure.[22,23] Aluminum oxide 90 standardized (Merck) was used for column chromatography. Organic solvents and mineral acids were of reagent grade and were used as supplied. Water was deionized and further purified by passage through a Elgastat UHQII (Elga) ion-exchange cartridge system (resistivity 18 MΩ cm).

[Cu(L¹H$_{-1}$)]ClO$_4$·H$_2$O. L¹ (300 mg, 0.90 mmol) dissolved in 20 mL of methanol was added dropwise to a stirred solution of $CuClO_4 \cdot 6H_2O$ (337 mg, 0.91 mmol) in methanol (10 mL). The initially green color of the reaction mixture progressively evolved to purple-red during stirring at room temperature. After 4 days, the solution was filtered and the solvent evaporated to dryness in vacuo. The residue was dissolved in water and the solution let to stand until violet-red, X-ray-quality crystals deposited in 50% yield (231 mg). IR (KBr): ν_{max} = 3580 (ν_{OHasym}), 3511 (ν_{OHsym}), 3117 (ν_{NH} bound), 3080 (ν_{CH} Ar), 2923 (ν_{CH_2}), 2876 (ν_{CH_2}), 1666 ($\nu_{C=O}$ amide), 1581 ($\nu_{C=O}$ amidate), 1535 (δ_{CNH}), 1465−1417 ($\nu_{C=C}$ + $\nu_{C=N}$ Ar), 1114 (ν_3 ClO_4^-), 1093 (ν_3 ClO_4^-), 624 cm^{-1} (ν_4 ClO_4^-). Anal. Calcd (found) for $C_{17}H_{24}N_5O_2CuClO_4 \cdot H_2O$: C, 39.93 (40.29); H, 5.12 (5.10); N, 13.69 (13.84).

[Cu(L¹H$_{-2}$)]·4H$_2$O. A solution of **L¹** (1.19 g, 3.59 mmol) and Na_2CO_3 (380 mg, mmol) in methanol (50 mL) was added dropwise to a stirred solution of anhydrous $CuCl_2$ (484 mg, 3.60 mmol) dissolved in methanol (50 mL). The mixture was refluxed for 12 h. After filtration, the solvent was evaporated in vacuo and the residue purified by column chromatography on alumina using CH_2Cl_2/CH_3OH (96/4 v/v) as eluent. A cyan-blue complex was isolated after crystallization in CH_3CN in 90% yield (1.4 g). (+) MALDI-TOF MS: m/z = 330.8 $[\mathbf{L^1}]^{+\bullet}$, 392.9 $[Cu(\mathbf{L^1}H_{-2})]^{+\bullet}$. IR (KBr): ν_{max} = 3430 (ν_{OH}), 3250 (ν_{OH}), 3079 (ν_{CH} Ar), 2962 (ν_{CH_2}), 2928 (ν_{CH_2}), 2850 (ν_{CH_2}), 1655 (δ_{HOH}), 1555 ($\nu_{C=O}$ amidate), 1458 ($\nu_{C=C}$), 1419 cm^{-1} ($\nu_{C=N}$ Ar). Anal. Calcd (found) for $C_{17}H_{23}N_5O_2Cu \cdot 4H_2O$: C, 43.91 (44.04); H, 6.72 (6.77); N, 15.06 (14.82).

Physical and Spectroscopic Measurements. Microanalyses were performed on a Fisons EA 1108 CHNS instrument. MALDI-TOF mass spectra were obtained on a Bruker ProFLEX III spectrometer using dithranol as matrix. Infrared spectra were measured on a Bruker IFS 66v Fourier transform spectrophotometer as KBr pellets from 4000 to 400 cm^{-1}. Low-temperature (100 K) X-band EPR spectra were recorded at the "Centre de Spectroscopie Moléculaire de l'Université de Bourgogne" in frozen water/ethylene glycol (7/3 v/v) mixed solutions on a Bruker ESP 300 spectrometer operating at ∼9.6 GHz equipped with a Bruker ER 4105 DR double cavity and a ER 4111 VT variable-temperature control unit. Instrumental settings were as follows: modulation frequency, 100 kHz; modulation amplitude, 1 mT; microwave power, 63 mW. A tube containing *N*,*N*′-diphenylpicrylhydrazyl (DPPH), used as an external calibration standard (g = 2.0037(2)), was introduced in the front cavity.

UV−Vis Spectroscopy. Electronic absorption and diffuse reflectance spectra were collected with a uniform data point interval of 10 cm^{-1} on a Cary 500 (Varian) spectrophotometer using either 1 cm quartz cells (Hellma) or a Labsphere DRA-CA-50 integration sphere. Samples for measurements in the solid-state were prepared by grinding ca. 5−10 mg of the pure complex with 300 mg of dry barium sulfate (Avocado, <99%) and the resulting powder was introduced in a homemade sample holder. Baseline corrections were applied by subtracting the residual noise recorded for pure barium sulfate from the signal. A Spectralon standard was used as reference cell. Corrected reflectance data (R) were then converted to $f(R)$ values using the Kubelka−Munk function ($f(R) = (1 - R)^2/2R$). Spectral deconvolution into Gaussian components was performed with the commercial software Origin 6.0 from Microcal[94] that uses a nonweighted, Marquardt nonlinear least-squares fitting procedure. Simulated profiles were iteratively refined with the fewest possible number of Gaussian bands to resolve the electronic d−d transitions contributing to the observed envelopes. The major problem associated with band deconvolution of overlapping components is that many different fits can be obtained for a single spectral data set, corresponding to local minima in the error hypersurface. To overcome this difficulty, various initial models differing in their band positions and bandwidths were iteratively adjusted to achieve both the optimal agreement factor and a random distribution over the entire wavelength range of the residual optical densities, which must be consistent with the instrumental noise level.

Thermal Analysis. Thermogravimetric (TGA) and differential thermal analysis (DTA) investigations were performed on a Netzsch STA 409 PC Luxx thermoanalyzer connected via a heated (ca. 200 °C) stainless steel capillary to GasLab 300 (VG-Gas) mass spectrometer controlled with the GasWorks 1.0 for Windows software. Samples purged in an argon (20 mL min^{-1})/dioxygen (10 mL min^{-1}) stream were heated to 1000 °C in alumina crucibles with a heating rate of 5 °C min^{-1}. Data were corrected for buoyancy effects. Onset temperatures (T_{onset}) were calculated according to the norm ISO 11357-3 as the intersection between the tangent in the inflection point and the selected baseline.

X-ray Crystallographic Data Collection. Selected crystals were mounted with silicon grease on the tip of a glass capillary. Diffraction data were collected at T = 110(2) K on a Nonius KappaCCD diffractometer,[95] equipped with a nitrogen jet stream

(94) *Origin 6.0*; Microcal Software Inc.: Northampton, MA.

low-temperature system (Oxford Cryosystems). The X-ray source was graphite-monochromatized Mo Kα radiation (λ = 0.710 73 Å) from a sealed tube. Lattice parameters were obtained by a least-squares fit to the optimized setting angles of the entire set of collected reflections. Intensity data were recorded as φ and ω scans with κ offsets. No significant intensity decay or temperature drift was observed during the data collections. Data reductions were done by using the DENZO software,[96] without applying absorption correction. The structures were solved by direct methods using either SIR92[97] or SHELXS97[98] programs. Refinements were carried out by full-matrix least squares on F^2 using the SHELXL97 program[99] and the complete set of reflections. Anisotropic thermal parameters were used for non-hydrogen atoms. Hydrogen atoms were refined with isotropic thermal factors constrained to 1.2 times the equivalent isotropic thermal factor of their respective bonded atom. The H(−C) hydrogen atoms were placed at calculated positions using a riding model, while the amidic H(−N) hydrogen atoms as well as those belonging to the cocrystallized water molecules H(−Ow) were located in the Fourier synthesis and their positional parameters refined. Relevant experimental crystal data and refinement details are summarized in Table 1. Molecular drawings were generated with the ORTEP-3 for Windows program.[100] Least-squares planes were computed with the PARST routine[101,102] included in WinGX crystallographic software package.[103] Structural similarity comparisons were performed with Chem3D from CambridgeSoft Corp.

[Cu(L^{1}H$_{-1}$)]ClO$_4$·H$_2$O. Red single-crystals were obtained by slow evaporation from an aqueous solution of the complex. A high-quality specimen of prismatic shape (0.24 × 0.20 × 0.18 mm^3) was selected for the diffraction experiment. A total number of 13 042 reflections were collected in the θ angle range 1.85−33.29°, which were reduced to 7067 unique reflections after merging. The Friedel pairs were not merged to estimate the Flack parameter. Its value at the final stages of the minimization was 0.07(1). Thus, a twinned crystal refinement was undertaken until the least-squares procedure converged to the final statistical agreement factors R1 = 0.0461 and 0.0508 for $I > 2\sigma(I)$ and all data, respectively.

[Cu(L^{1}H$_{-2}$)]·4H$_2$O. Blue single-crystals were obtained by slow evaporation from a solution of the complex in a $CH_3CN/C_2H_5NO_2/N(C_2H_5)_3$ mixture. A high-quality specimen of prismatic shape (0.20 × 0.18 × 0.10 mm^3) was selected for the X-ray diffraction experiment. A total number of 11 132 reflections were collected in full θ range 1.96−30.06° and merged into 5858 independent reflections. The positional parameters of the hydrogen atoms belonging to the cocrystallized water molecules were refined with restrained Ow−H distances (0.96 Å) and H−Ow−H angles (107°). The structure showed a disordered ligand molecule around the metal center, involving mainly the 14-membered macrocyclic fragment and the methylenic carbon atoms from the strap. In fact, two conformers with site occupation factors of 0.765(4) and 0.235(4), respectively noted A and B, were found to be superimposed. The following pairs of atoms share the same sites: (C3A, C12B); (C3B, C12A); (N4A, N11B); (N4B, N11A); (C5A, C10B); (C5B, C10A). The atomic pyridine-ring positions were found to be identical for both conformers.

Spectrophotometric Titrations. Potentiometric titrations coupled with a spectrophotometric detection were carried out at constant ionic strength (I = 0.1 M, KNO_3) and temperature (25.0(1) °C) in a jacketed titration vessel maintained under an argon atmosphere and fitted to a Lauda RE 106 water circulator. A glass-bulb XG100 (Radiometer-Tacussel) electrode was used together with a XR110 (Radiometer-Tacussel) KCl-saturated calomel electrode, the latter being separated from the bulk of the solution by a sintered-glass bridge filled with a 0.1 M KNO_3 solution. Prior to each titration, the electrochemical cell was calibrated to read hydronium ion concentrations (p[H] = −log [H_3O^+]). The detailed procedure and equipment have been described in detail elsewhere.[1]

Visible absorption spectra of the copper complexes as a function of p[H] were recorded in-situ with a Cary 50 Probe (Varian) spectrophotometer equipped with an immersion cell (Hellma, ref 661.202) of 1 cm path length made of quartz (SUPRASIL 300). Both 2-m-long built-in light guides of the dip probe were directly connected through SMA plugs to the coupling device, fitted inside the sample compartment of the spectrometer. Prior to the titration, the reference spectrum of the supporting electrolyte solution was acquired in the 400−900 nm range. The standard deviation of the measured absorbance for the baseline was constant over the entire wavelength region and did not exceed 0.001 absorbance unit. Aliquots of a standardized 0.1 M KOH solution were added manually with the help of a Gilmont micropipet (2 μL resolution). The potential of the calibrated glass electrode was measured with a PHM240 (Radiometer-Tacussel) ionometer. Enough time was allowed after the addition of each base increment to reach the equilibrium. The potential-drift criterion was set at dE/dt < 0.1 mV min^{-1}. The collection of absorption spectra was repeated with 2 min delays between two consecutive measurements until superimposable spectra were obtained with optical densities not exceeding 0.5 units. For each titration point, the pH-meter readings were stable in less than 2 min and no more than two spectral recordings were required.

The multiwavelength data sets were decomposed into their principal components by factor analysis with the SPECFIT program.[89−91] The stability constant and the extinction coefficients corresponding to each species were subsequently adjusted to the reduced data sets by the Marquardt nonlinear least-squares algorithm. Furthermore, the data from each titration were also processed by the program HYPERQUAD 2000, which allows the simultaneous treatment of potentiometric and spectrophotometric data.[88] While SPECFIT converts directly the measured p[H] values to the free H_3O^+ concentrations, the mass-balance equations for all components, including the hydronium ion, are solved at each titration point by the program HYPERQUAD. Since the precision of spectrophotometric and potentiometric measurements is different, it is essential to define a proper weighing scheme relying on the error-propagation rule that gives to each type of observations an approximately equal contribution to the residual sum of squares. Realistic parameter estimates of the quadratic absorbance error function ($\sigma_A = a + bA + cA^2$) were evaluated by computing for each recorded wavelength of 50 replicates of the ligand spectrum, the average absorbance and its associated standard deviation.[88,104] The selected weighing-scheme seeks also to reduce the weight of the less accurate measurements (i.e. points located in the steep region of a titration curve). On the basis of the instrument's

(95) *COLLECT, Data Collection Software*; Nonius, BV: Delft, The Netherlands, 1998.
(96) Otwinowski, Z.; Minor, W. *Methods Enzymol.* **1997**, *276*, 307.
(97) Altomare, A.; Cascarano, G.; Giacovazzo, C.; Guagliardi, A. *J. Appl. Crystallogr.* **1993**, *26*, 343.
(98) Sheldrick, G. M. *SHELXS-97, Program for the Solution of Crystal Structures*; University of Göttingen: Göttingen, Germany, 1997.
(99) Sheldrick, G. M. *SHELXL-97, Program for the Refinement of Crystal Structures*; University of Göttingen: Göttingen, Germany, 1997.
(100) Farrugia, L. J. *J. Appl. Crystallogr.* **1997**, *30*, 565.
(101) Nardelli, M. *Comput. Chem.* **1983**, *7*, 95.
(102) Nardelli, M. *J. Appl. Crystallogr.* **1995**, *28*, 659.
(103) Farrugia, L. J. *J. Appl. Crystallogr.* **1999**, *32*, 837.
(104) Gans, P. *Data Fitting in the Chemical Sciences*; Wiley: Chichester, U.K., 1992.

calibration, the uncertainties associated with the experimental p[H] values (σ_{pH}) and the volumes delivered by the piston buret (σ_v) were estimated as 0.003 pH unit (or ~0.1 mV) and 0.005 mL, respectively. The fit between calculated and experimental data was evaluated through the squared sum of residuals ($1.2 < \sigma < 1.75$) and an approximately normal distribution of the residues.[104] The thermodynamic reversibility was checked by cycling from low to high p[H] and vice versa. Data from forward and backward titrations afforded statistically identical values of the adjusted thermodynamic parameters.

Electrochemistry. Cyclic voltammetry was carried out in absolute acetonitrile solutions containing 0.1 M $[N(n\text{-}C_4H_9)_4]ClO_4$ (TBAP) as supporting electrolyte (Aldrich) with an EG&G model 173 potentiostat. A three-electrode system was used and consisted of a glassy carbon or platinum disk working electrode, a platinum wire counter electrode, and a saturated calomel reference electrode (SCE). The SCE was separated from the bulk of the solution by a fritted-glass bridge of low porosity, which contained the solvent/supporting electrolyte mixture. All potentials are referenced to the SCE.

Spectroelectrochemistry. UV−vis spectroelectrochemical experiments were performed with an optically transparent platinum thin-layer electrode of the type described in the literature.[105] Potentials were applied with an EG&G model potentiostat. Time-resolved UV−vis spectra were recorded with a Hewlett-Packard model 8453 diode array rapid-scanning spectrophotometer. Infrared spectra were recorded on an FTIR Nicolet Magna-IR 550 spectrometer. The background was obtained by recording the IR spectrum of the neutral compound under N_2.

Acknowledgment. This work was supported by the Centre National de la Recherche Scientifique (CNRS), the Conseil Régional de Bourgogne, and the R. A. Welch Foundation (K.M.K.; Grant E-680). L.F. thanks the Ministère de l′Education Nationale de la Recherche et de la Technologie for a Ph.D. scholarship. Dr. Stéphane Brandès is also gratefully acknowledged for his experimental assistance with the TGA measurements and helpful discussions.

Supporting Information Available: Cyclic voltammograms in the cathodic region of $[Cu(\mathbf{L^1}H_{-1})]ClO_4 \cdot H_2O$ and X-ray crystallographic files in CIF format for the structure determinations. This material is available free of charge via the Internet at http://pubs.acs.org.

IC049518K

(105) Lin, X. Q.; Kadish, K. M. *Anal. Chem.* **1985**, *57*, 1498.